Precambrian Research 338 (2020) 105568

Contents lists available at ScienceDirect

Precambrian Research

journal homepage: www.elsevier.com/locate/precamres

The architecture of the Buem Structural Unit: Implications for the tectonic evolution of the Pan-African Dahomeyide Orogen, West Africa

Daniel Kwayisi*, Jérémie Lehmann, Marlina Elburg

Department of Geology, University of Johannesburg, Auckland Park Kingsway Campus, Johannesburg, South Africa

ARTICLE INFO

Keywords:
Aeromagnetic
Collision
Structural geology
Accretion
Fold and thrust belt
Pan-African orogeny

ABSTRACT

The Buem Structural Unit (BSU) occurs about 50 km west of the high-pressure (HP) rocks of the Pharusian suture zone (PSZ) of the Dahomeyide Orogen, West Africa. Shale and sandstone intercalations form the base of the BSU, followed by serpentinised peridotite, gabbro, massive and pillow basalts (fragment of oceanic crust), jasper/chert, and limestone/dolostone, with sandstone and diamictite forming the top of the BSU. The package was deformed at lower greenschist-facies conditions during the Pan-African orogeny. The N-S-trending BSU has been affected by three deformational events. The main deformation event D2, which transposed bedding-parallel D1 fabrics, produced a steeply ENE-dipping S2 tectonic foliation. S2 is axial planar to upright or west-verging isoclinal and chevron F2 folds. Top-to-the-west D2 shear zones in the sandstone, shale and serpentinised peridotite are associated with a down-dip ENE-plunging L2 stretching lineation. The mafic-ultramafic rocks occur as D2 tectonic slices, marking the boundaries between thrust sheets within the BSU. The D2-related N-S trending structural and short-wavelength (< 1 km) magnetic grain of the BSU is superimposed on ENE-trending long-wavelength (> 1 km) magnetic anomalies that are continuous along trend with the regional structures of the West African Craton (WAC) and are interpreted as signals from the basement rocks of the BSU. D2 deformation is interpreted to result from overthrusting of the BSU onto the southeastern margin of the WAC during collision of the WAC and Benino-Nigerian Shield (BNS). Meter-scale, steep and open F3 kink and crenulation folds with steeply SE-dipping axial planes are sporadically observed throughout the entire BSU. D3 deformation is inferred to reflect a period of NW-SE-shortening. Deformation history of the BSU shares structural similarities with the one of the PSZ. We, therefore, interpret the BSU as an allochthonous fold and thrust belt with a geodynamic evolution involving subduction of the WAC beneath the BNS and the ensuing collision between the two terranes. The tectonic framework of the BSU suggests a geodynamic evolution of the Dahomeyide Orogen evolving from initial accretion of oceanic crust and deposition of passive margin sedimentary sequences, and their inversion due to continent-continent collision during the Pan-African orogeny.

1. Introduction

The Dahomeyide Orogen, along the southeastern margin of the West African Craton (WAC) comprises passive and active margin units, ultrahigh to high pressure (UHP-HP) oceanic terranes, basement complexes and post-collisional sedimentary basins (e.g. Attoh, 1998; Ganade de Araujo et al., 2014; Guillot et al., 2019). The Dahomeyide Orogen formed during the Pan-African orogeny and assembly of NW Gondwana between 780 and 540 Ma (Ganade de Araujo et al., 2014, 2016), related to the subduction of an oceanic basin, the Pharusian Ocean, followed by continental subduction of the WAC, and continent-continent collision with the Benino-Nigerian Shied (BNS; e.g. Attoh, 1998; Attoh et al., 2006; Agbossoumondé et al., 2002, 2004; Duclaux et al., 2006; Ganade de Araujo et al., 2014, 2016; Guillot et al., 2019).

The Buem Structural unit (BSU) in Ghana is represented by weakly metamorphosed fragments of oceanic lithosphere (Burke and Dewey, 1972; Affaton et al., 1997; Asiedu et al., 2008; Nude et al., 2015) associated with passive margin and continental sedimentary units (Jones, 1990; Affaton et al., 1997; Nude et al., 2015). A well-defined suture, the Pharusian suture zone (PSZ), is marked by the occurrence of eclogite and granulite gneisses, some 50 km east of the BSU. This belt of UHP-HP rocks was exhumed during E-W oceanic closure involving continental subduction at ca. 620–605 Ma (Affaton et al., 2000; Hirdes and Davis, 2002; Guillot et al., 2019). The BSU is separated from the PSZ by a discontinuous belt of Paleoproterozoic mylonitic granitoid gneisses (locally referred to as the Ho-gneisses, e.g. Attoh 1998; Attoh et al.,

* Corresponding author.
E-mail addresses: danielk@uj.ac.za, 217039544@student.uj.ac.za (D. Kwayisi).

https://doi.org/10.1016/j.precamres.2019.105568
Received 26 August 2019; Received in revised form 7 December 2019; Accepted 9 December 2019
Available online 19 December 2019
0301-9268/

2007) and the metasedimentary rocks of the Togo Structural unit (TSU; Ghana National Geological Map Project, 2009). How the BSU, a domain of at least partial oceanic affinity, but physically separated from the PSZ units, relates to the formation of the orogenic belt remains enigmatic. For instance, Jones (1990) suggested that the BSU formed during rifting of continental crust and was not affected by the Pan-African collision. On the contrary, Affaton et al. (1997) indicated that the BSU underwent a major thrusting event under both ductile and brittle conditions. These different interpretations are mainly due to the poor documentation of the lithostratigraphic sequence and structural relations of the various units within the BSU and the lack of detailed structural and petrological studies.

This paper presents for the first time high-resolution magnetic and radiometric data for the entire Ghanaian portion of the BSU. These are used to review the surface and deep crustal architecture of this belt. The total magnetic intensity and radiometric data have been interpreted in conjunction with the existing 1:1,000,000 scale geological map, a digital elevation model using Shuttle Radar Topography Mission (SRTM 3; 30 m spatial resolution) data, and field data. In addition, this paper describes the deformation history of the BSU in order to provide constraints on its tectonic evolution in the framework of the geodynamic evolution of Pan-African Dahomeyide Orogen of West Africa.

2. Geological setting

The WAC stabilised tectonically after the last main phase of the Eburnean orogeny at ca. 2000 Ma (Schlueter, 2005; Petters, 2014). The WAC is surrounded entirely by Pan-African Mobile Belts (Fig. 1a; Ennih and Liégeois, 2008). Among these is the Trans-Saharan mobile belt (of which the Dahomeyide Orogen is a part; Black et al., 1979, 1994; Affaton et al., 1991; Attoh and Nude, 2008), which occurs at the eastern margin of the WAC. The Anti-Atlas, Rockelide, and Bassaride/Mauritanide belts occupy the northern, southern, and western margins of the WAC (Villeneuve and Dallmeyer, 1987; Hefferan et al., 2000; Ennih and Liegeois, 2001). The WAC in Ghana consists of alternating ENE-trending greenstone and metasedimentary belts of the Birimian Supergroup (Fig. 1b) assembled at ~2.1 Ga during the Eburnean orogeny, intruded by Eburnean granitoids, and overlain by the slightly younger clastic sedimentary rocks of the Tarkwaian Group. The sedimentary rocks of the ca. 900 to 450 Ma Voltaian Supergroup occupy the southeastern part of the WAC and border the Dahomeyide Orogen to the west (Fig. 1b).

In Ghana, Togo and Benin, the southern segment of the long (> 2500 km) Trans-Saharan mobile belt is exposed as the Dahomeyide Orogen (Fig. 1a, e.g., Trompette, 1997; Ganade de Araujo et al., 2014). This orogen resulted from the eastward subduction of Neoproterozoic passive margin sequences and Pharusian oceanic crust, and subsequent collision of the WAC with the BNS (Attoh, 1998; Castaing et al., 1993; Agbossoumonde et al., 2004; Duclaux et al., 2006; Attoh et al., 2013). The Dahomeyide Orogen is separated from the Paleoproterozoic Birimian rocks and the Voltaian Supergroup by the generally N-S trending, west-verging Pan-African frontal thrust, (Fig. 1b; Ghana National Geological Mapping Project, 2009). Three structural units have been identified within the Dahomeyide Orogen, namely, the Buem, Togo and Dahomeyan structural units (from west to east on Fig. 1b; Attoh, 1982; Ghana National Geological Mapping Project, 2009). The Buem and the Togo structural units are part of the external zone, whereas the Dahomeyan Structural Unit comprises the suture, the internal zones, and a part of the external zone (Ho-gneisses). These three zones possess distinct gravity anomalies (El-Hadj Tidjani et al., 1997). The external zone is characterised by a negative isostatic anomaly interpreted to reflect the presence of a crustal root. The suture and internal zones feature strong positive anomalies, which are connected with heavy deep structures, interpreted to correspond to a root of basic rocks, e.g. an underplated fore-arc (Guillot et al., 2019).

The Togo Structural Unit (TSU) and the Voltaian Supergroup border the BSU to the east and west, respectively (Fig. 1b). Rocks of the BSU extend from Ghana through to Togo and Benin, and form a belt that is about 750 km long and 5–50 km wide (Affaton, 1990; Affaton et al., 1997). The BSU consists of sedimentary, volcanic and mafic-ultramafic plutonic rocks (e.g. Affaton, 1990; Jones, 1990; Affaton et al., 1997; Nude et al., 2015; Kwayisi et al., 2017). Detrital zircon ages of the sediments of the BSU indicate that two main sources exist. A population with the youngest zircons dated at ~950–1000 Ma correlates with the lower part of the Voltaian Supergroup and is interpreted as passive margin deposits of the Pharusian Ocean (Kalsbeek et al., 2008). A younger population with detrital zircons as young as ~600 Ma correlates with the middle Voltaian Supergroup sediments and is interpreted as foreland deposits shed from the eastern internal units after collision (Ganade de Araujo et al., 2016). Recent work by Nude et al. (2015) and Kwayisi et al. (2017) has focused on the volcanic and associated mafic–ultramafic plutonic rocks of the BSU (Fig. 1c). The volcanic rocks are mainly alkali and subalkaline basalts, basaltic-andesite and trachyte (Nude et al., 2015) associated with pyroclastic rocks and volcanic breccias (Kwayisi, 2014; Kwayisi et al., 2017). The mafic–ultramafic plutonic rocks are gabbro and serpentinised peridotite (Kwayisi et al., 2017). There is little agreement on the stratigraphy of the BSU in the literature (Table S1 of Supplementary data), because of folding and thrust faulting, and because different authors focused on different parts of the BSU.

Affaton et al. (1997) described the Buem volcanic rocks in the Tiele area, NW Benin (Fig. 1c) as having undergone extension-related metamorphism, under prehnite-pumpellyite facies conditions. These authors reported later mineralogical re-equilibration under slightly higher pressure pumpellyite-actinolite facies, associated with burial during the Pan-African orogeny, but without noticeable temperature increase. In Ghana, lower greenschist facies metamorphism (chlorite, epidote, and albite) is inferred from the volcanic rocks and the sandstones (Jones, 1990; Nude et al., 2015). The BSU was deformed by west-verging imbricated thrust systems and duplexes (Affaton, 1990; Affaton et al., 1997). The thrust sheets are rarely associated with the occurrence of serpentinite (Wright et al., 1985; Griffis et al., 2002). Jones (1990) identified two NE-SW striking main faults (North and South Nkonya) that are located between Kpandu and Fudome (Fig. 1c). Nude et al. (2015) suggested that the volcanic rocks have been displaced to the east by the North Nkonya fault. The inferred offset of the top of the volcanic rocks across the north and south faults implies a dextral displacement on the southern fault and a sinistral displacement on the northern fault (Jones, 1990).

3. Field relations and structures

The BSU features several broadly N-S trending ridges and valleys, which are strongly influenced by the lithological units. Detailed field mapping has highlighted the occurrence of sedimentary (clastic and chemical), volcanic and mafic–ultramafic plutonic rocks within the BSU (Table 1). Fig. 2 presents the tectono-stratigraphic column of the BSU, which will be discussed from bottom to top. Structurally, slate, schist, and arkosic sandstone occupy the base of the BSU, followed progressively upwards by peridotite, gabbro, and massive and pillow lavas, turbiditic shale/greywacke and chemical sediments, with quartz-rich, diamictite, and volcaniclastic sandstone forming the upper part of the BSU (Fig. 2). The sandstone, diamictite and occasionally ironstone make up the ridges with the shale occupying the valleys and lowlands. The volcanic, mafic and ultramafic plutonic rocks, jasper, chert, and limestone/dolostone also form ridges; however, they are not as prominent as the sandstone ridges.

The slate and schist are strongly folded and foliated (with the growth of chlorite and muscovite); schistosity is best developed especially at the contact with the igneous rocks. The slate is occasionally intercalated with sandstone (Fig. 3a). The peridotite has undergone various degrees of serpentinisation, brecciation and schistosity

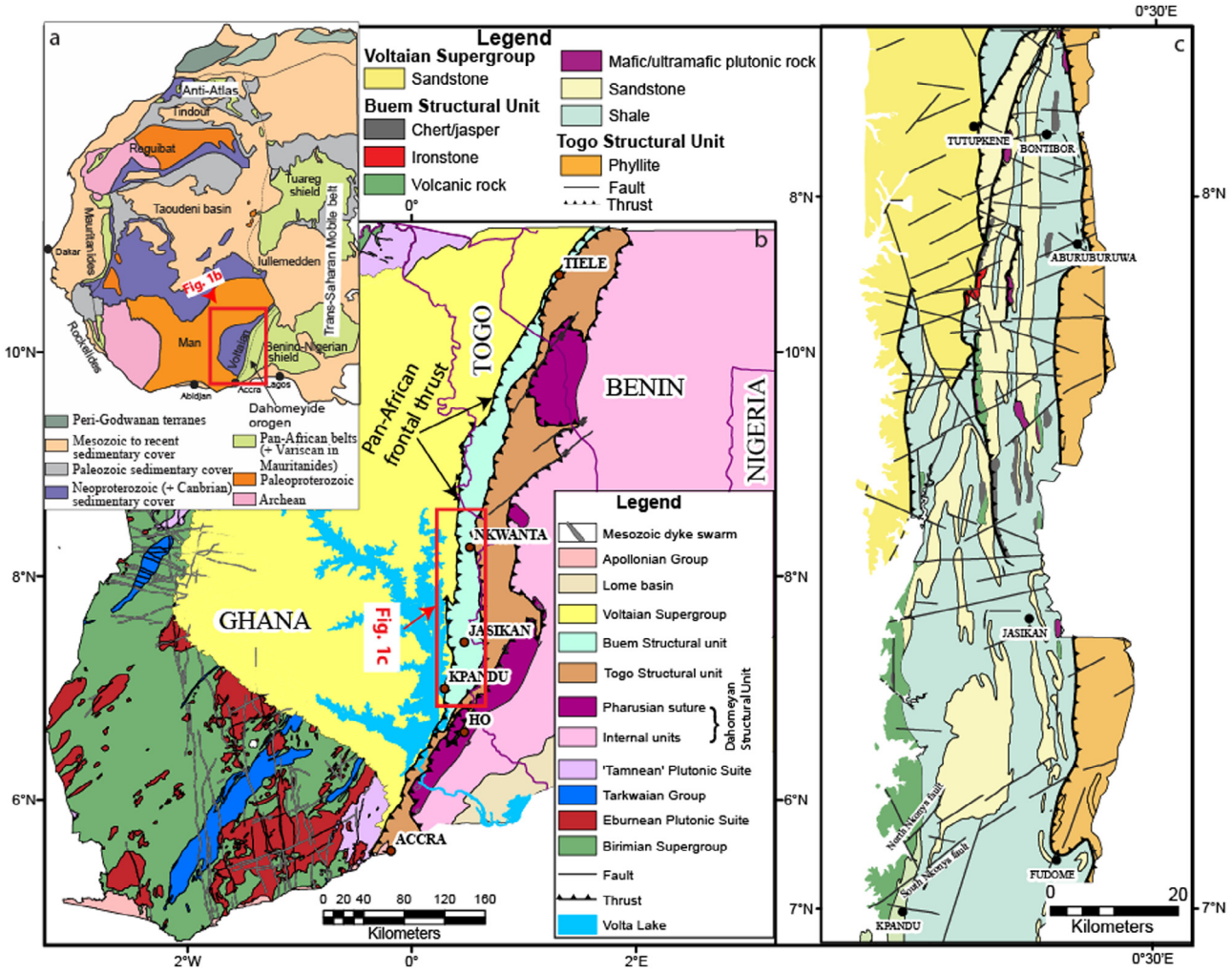

Fig. 1. (a) Simplified tectonic map of the West African craton and surrounding Pan-African and Hercynian orogenic belts (modified after Ennih and Liégeois, 2008). (b) Geological map of the Pan-African orogenic belt in Ghana, Togo and Benin and adjoining Paleoproterozoic Birimian rocks to the west. Note the internal crustal architecture of the WAC in Ghana marked by ENE-trending belts. (c) Geological map of the Buem Structural Unit (extracted from the 1,000,000 geological map of Ghana, 2009).

development (Fig. 3b) but its primary cumulate texture, is well-preserved in many places. The peridotite units are typically overlain by the gabbro with a tectonic contact. In places, a thin layer (about 2 m) of limestone/dolostone overlies the peridotite with a primary contact (e.g. near Aburubuwa, Fig. 3b). Primary contacts between gabbro and volcanic rocks are locally preserved, suggesting a shared pre-deformation geological history. However, in most places, the gabbro shows schistosity (Fig. 3c) marked by chlorite and epidote, and structurally underlie the volcanic rocks with a tectonic contact. The jasper/chert either occurs as a cm-thick veins within the pillow lavas or is interlayered with limestone/dolostone or massive beds overlying the volcanic rocks (Fig. 3d and 3e). This association may suggest the formation of the jasper/chert and limestone/dolostone in a marine environment.

The pillow lavas range in size from about 0.3 to 2 m with downward-pointing bases and rounded upper surfaces observed on horizontal pavement outcrops suggesting that the lavas have been steeply folded around a NNW-plunging axis (Fig. 3f). At the contact with the sedimentary and mafic–ultramafic plutonic rocks, the volcanic rocks are schistose with steep dips to the east or west (Fig. 3g). Thin layers (0.5 to 1 m) of reddish shale and sandstone, and turbiditic shale/greywacke sometimes occur within the volcanic rocks. These sedimentary rocks are deformed, showing elongation and preferred orientation of their framework grains. Massive and thick (0.5 to 1 m) beds characterise the sandstone and diamictite (Fig. 3h). Rock fragments within the diamictite include granitoids, metamorphic rocks (such as slate, schist, and quartzite), and fragments of sandstones, greywacke, and volcanic rocks. Thin (1 to 5 cm) layers of slate often occur as interbeds within the diamictite and sandstone.

Three tectonic foliations (S1, S2, and S3) are developed throughout the rocks of the BSU. The ubiquitously developed NNW-striking S2 foliation (Fig. 4a) is axial planar to isoclinal and chevron F2 folds that are cylindrical at mesoscale (Fig. 4a-c). S2 has folded an existing but poorly preserved bedding-parallel metamorphic planar fabric (S0-1; Fig. 4c). Poles to S2 planes broadly cluster along a WSW-ENE direction (Fig. 5a) which is compatible with shallow to sub-horizontal NNW-trending B2 fold axes (Fig. 5b, open diamonds). The moderate scattering in dip angle of the main metamorphic foliation in Fig. 5a is interpreted as fanning of S2 and/or not fully S2-transposed S0-1 foliations. S2 is marked by shape-preferred orientation of quartz, albite, chlorite, and muscovite in the slate and quartzite, and chlorite, epidote, and albite in the mafic volcanic and plutonic rocks, and serpentine in the ultramafic rocks (Fig. 4c and 4d). S2 is strongly developed in the slate and schistose peridotite and more weakly in the volcanic and schistose gabbro, jasper/chert, limestone/dolostone, and quartzite.

Locally-developed bedding- and S2-parallel shear zones range in length from 3 to 10 m and in width between 0.5 and 1 m (Fig. 6). Shear zone-bounded internal S2 schistosity is sigmodal in shape and associated with down-dip L2 slicken or stretching lineations (Fig. 5b, filled

Table 1
A summary of the major units of the BSU, their mineralogical composition, measured magnetic susceptibility properties, and general features on the geophysical maps.

Legend	Lithology and structures	Mineralogy	Susceptibility	Airborne magnetic response	Magnetic image	Airborne radiometric response	Radiometric image	Geological interpretation
Ultramafic	Peridotite, mainly harzbugite	Ol, Opx, Srp, Spl	16.1–54.5 × 10^{-3} SI	Moderate to high intensity, smooth texture, N-S magnetic trends(RTE)	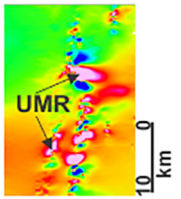	Very low K, eTh, eU content. Dark areas	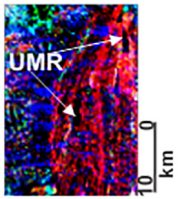	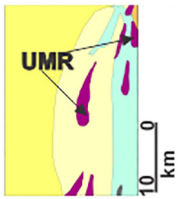
Mafic plutonic	Gabbroic rock	Cpx, Pl, Opx, Mag, Chl, Ep	0.32–106 × 10^{-3} SI	Indistinguishable from the ultramafic rocks (RTE)		Indistinguishable from the ultramafic rocks		
Lava flow	Alkali basalt, subalkaline basalt	Cpx, Pl, Ser, Chl Act	0.17–55.3 × 10^{-3} SI	Moderate to high intensity, Mottled texture (RTE)	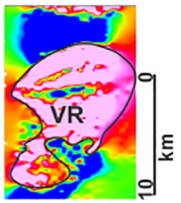	Very low K, eTh, eU content. Dark areas	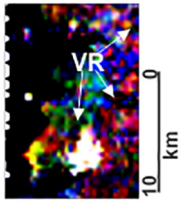	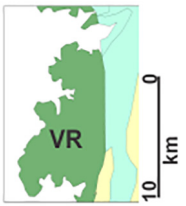
Pyroclastics	Agglomerate, pyroclastic breccia, hyaloclastite	Cpx, Pl, Cb	0.32–17 × 10^{-3} SI	Moderate to high intensity, similar to the lava flow (RTE)		Very low K, eTh, eU content. Dark areas		
Sedimentary rocks	Sandstone, chert/ jasper, diamictite	Qz, Pl, Ksp, Ms, Chl, Cb	0.11–0. 22 × 10^{-3} SI	Low to moderate intensity, smooth texture (RTE)	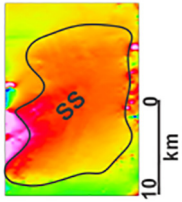	Moderate to high K, low eTh, and eU content. Magenta areas	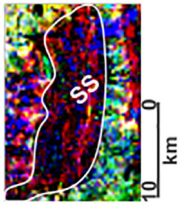	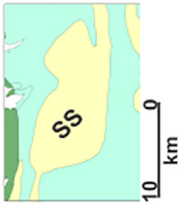
	Shale	Ser, Ms, Chl, Qz	0.012–1.31 × 10^{-3} SI	Low to moderate intensity, smooth texture, uniform (RTE)	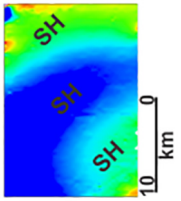	Moderate to high K, eTh, and eU content. Whitist green areas	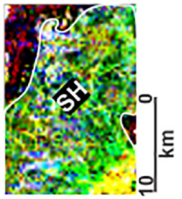	
Thrust fault				Cyclic repetition of same magnetic signal and asymmetric sharp changes in magnetic pattern (1VD)	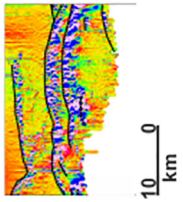	Changes in radio-element content when contrasting lithologies are present	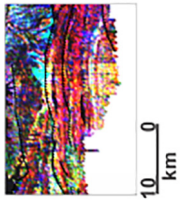	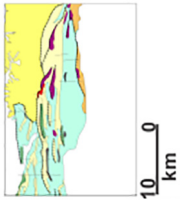

Note: Scale bar (thick black line) is 10 km. UMR = ultramafic rock, VR = volcanic rock, SS = sandstone, and SH = shale. Mineral abbreviation after Whitney and Evans (2010). Act = actinolite, Cb = carbonate mineral, Chl = chlorite, Cpx = clinopyroxene, Ep = epidote, Ksp = K-feldspar, Mag = magnetite, Ms = muscovite, Ol = olivine, Opx = orthopyroxene, Pl = plagioclase, Qz = quartz, Ser = sericite, Spl = spinel, Srp = serpentinite.

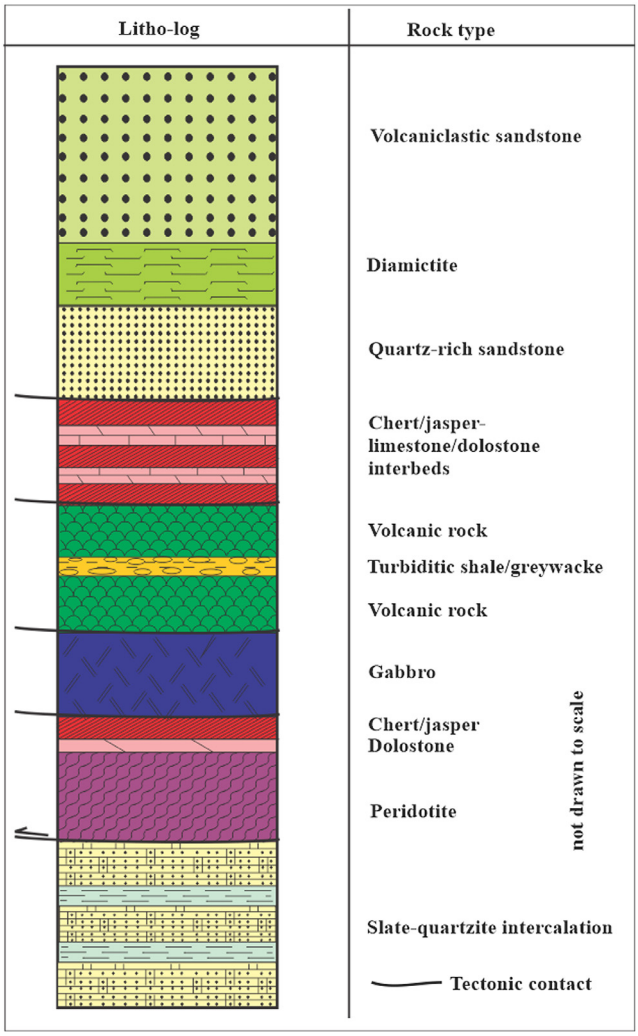

Fig. 2. Tectono-stratigraphic sequence of the BSU, showing primary and secondary relationships between the different units. Thick lines in-between units represent tectonic contacts, whereas faint lines represent primary or stratigraphic contacts.

diamonds).

F3 kink bands, crenulations, and S-type folds (Fig. 3f, 4e, and 4f respectively) exhibit sub-vertical to steeply SE-dipping axial planes (Fig. 5c, filled squares), parallel to locally developed S3 tectonic foliation. B3 fold axes are shallowly to steeply ENE-plunging; the spread representing the variation in orientations of the folded S2 foliation (Fig. 5c, open squares).

4. Geophysical data and processing

4.1. Geophysical data

The Geological Survey Authority of Ghana (GSA), in partnership with the Geological Survey of Finland (GKT) and the Minerals Commission of Ghana, acquired the airborne geophysical data between 1997 and 1998. During the aeromagnetic survey, a nominal flight line spacing of 400 m with a flying height of 70 m and a tie-line of approximately 5 km were maintained for the terrain. The survey was flown along an east–west direction (i.e., orthogonal to the main structural grain of the BSU) by means of a fixed-wing aeroplane (Cessna Titan 404 (C-FYAU)) with a resolution of 0.01 nT and a noise envelope of 0.1 nT. Measurements were taken every 8 m. Radiometric data sampling was done every 80 m using an aeroplane with Exploranium spectrometer (model GR-820) with 256 spectral channels and a GPX-1024 detector with 1024 cubic inches of NaI (Tl) (sodium iodide crystals treated with thallium) mounted on it. Real-time differential GPS was used for positioning. These data were integrated with SRTM 3, and with both published and our new geological and structural data for a better interpretation.

4.2. Data processing

Before detailed processing and transformation of the aeromagnetic and radiometric data, GKT performed the following corrections: diurnal variations, differences in terrain clearance, stripping, the lag error between the aeroplane and the sensor, instrument variation, discrepancies between flight lines and tie lines, aeroplane heading, micro-levelling, and background correction. The micro-levelling corrected the small inconsistencies and spatially homogenised the data and made it possible to generate a better image for analysis. The corrected Total Magnetic Intensity (TMI) and radiometric data were interpolated onto a square grid using a grid cell size of 100 m (Figs. 7–9 and Supplementary Fig. 1 and Supplementary Fig. 2).

4.2.1. Aeromagnetic data: Total magnetic intensity (TMI)

Milligan and Gunn (1997) and Guy et al. (2014) suggested that, since the appearance of a magnetic signal is heavily reliant on the inclination of the ambient geomagnetic field, the magnetic signals are asymmetric and are not centred above their causative bodies except at the magnetic poles where the magnetic field is vertical. As such, a commonly employed procedure is to transform the magnetic anomalies to that which would be observed in a vertical geomagnetic field and to centre them over their sources (Gunn, 1997). Mathematical transformation or filtering methods, such as Reduce-to-the-Pole (RTP) and analytic signal (AS), are usually applied to place the magnetic anomaly as if it sits over the magnetic source (Gunn, 1997). However, in areas of low magnetic inclination (i.e., areas close to the equator; inclination $< 15^{\circ}$) the traditionally performed RTP becomes unstable (MacLeod et al., 1993; Li, 2008). Also, N-S oriented anomalies could not be represented accurately at low inclinations (Beard, 2000; Reeves, 2005). Hence, in low magnetic inclination areas, the Reduce-to-the-Equator (RTE) or some modification of the RTP are applied (MacLeod et al. 1993; Li, 2008). The magnetic inclination for the BSU was found to be 12.5° thus the RTE transformation was applied to the gridded image (Fig. 8a).

In general, magnetic anomalies are always broader than the causative body, and this creates a problem of anomaly interference between adjacent bodies, causing the delineation of the edges of bodies to be very difficult. To resolve this and make qualitative interpretation easier, processing using the First Vertical Derivative (1VD) and the Analytical Signal (AS) was done (Fig. 8b and Supplementary Fig. 1a). 1VD is a good method for resolving anomalies in TMI maps by preserving peak amplitudes over the causative magnetic bodies while suppressing the regional magnetic field component (Paine, 1986). The 1VD reduces the width of anomalies and match more closely the source body. The AS technique is used to locate the edges of remanently magnetized bodies and to centre anomalies over their source bodies. This is based on the premise that the strength of magnetisation of rocks is directly proportional to their analytical signal. Oruc and Selim (2011) indicated that long-wavelength anomalies are not necessarily diminished when delineating linear features by applying edge delineation filters. Hence, a Tilt-Angle Derivative (TDR) filter was applied to enhance short-wavelength anomalies and expose the presence of magnetic lineaments (Fig. 8d). Upward continuation filtering aided in determining the depth range of deeper magnetic sources (Fig. 8c and 8d, and Supplementary Fig. 1c and Fig. 1d).

With the Depth-to-Basement extension on Geosoft Oasis Montaj, the depth-to-basement of the magnetic source was determined, employing Werner Deconvolution (WD). WD can determine the position and

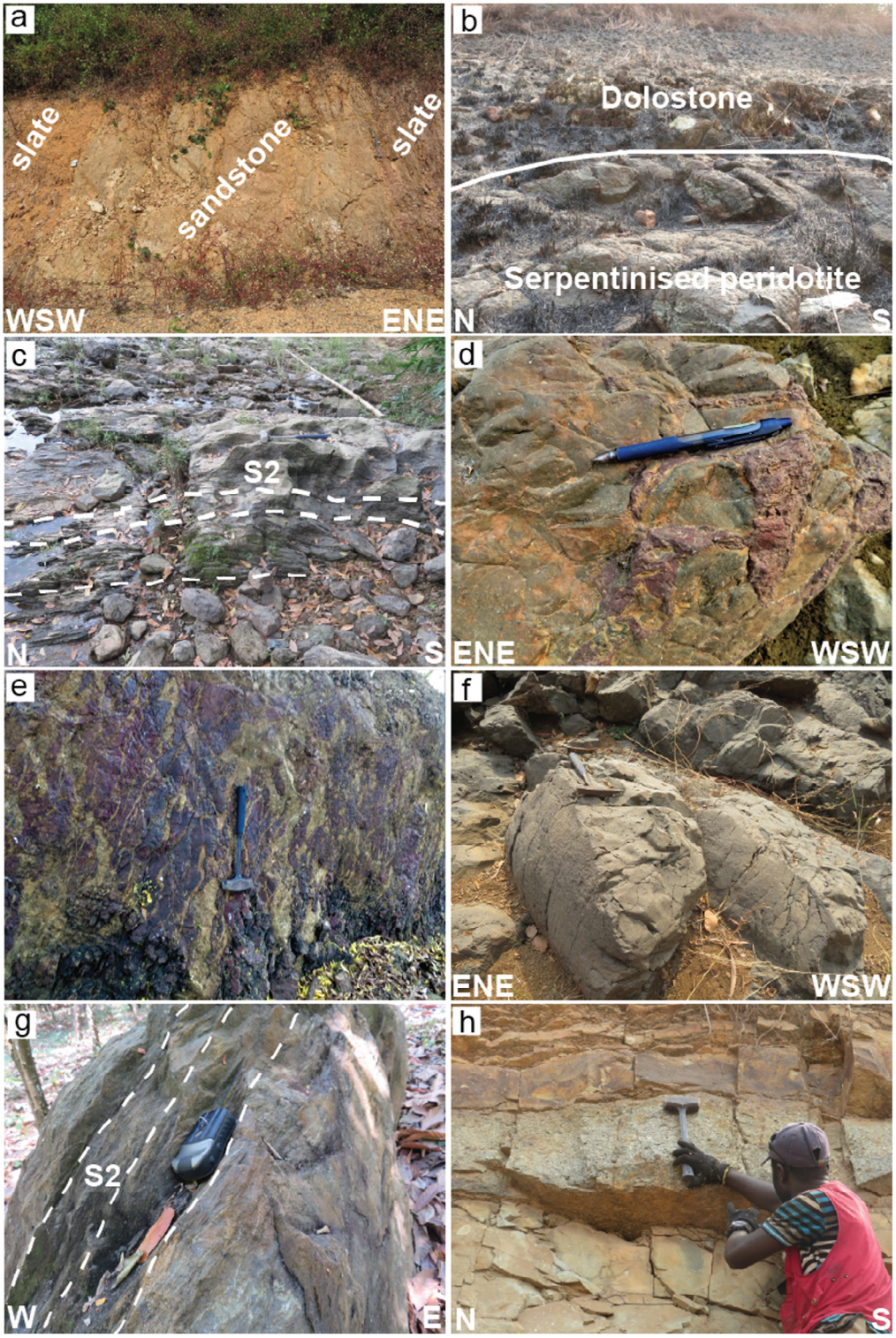

Fig. 3. Field photographs of (a) intercalation of slate and sandstone, (b) serpentinised peridotite in primary contact with dolostone, (c) schistose gabbro, (d) jasper vein cutting pillow lava (e) jasper-limestone interlayers, (f) pillow lava facing ENE, (g) schistose basalt, and (h) thick (> 30 cm) beds of sandstone and diamictite.

strength (i.e. magnetic susceptibility) of a magnetic causative body for a magnetic profile by using the horizontal and vertical derivatives and a least-squares approach (Ku and Sharp, 1983). The authors suggested that this method is particularly useful because the horizontal gradient of the total magnetic field produced by the edge of a wide tabular body is comparable to the total field from juxtaposed thin dykes. WD makes the assumption that the causative body were either dykes or contacts with unlimited depth range.

4.2.2. Radiometric data

The radiometric data were gridded and subjected to several enhancing techniques for better understanding of the radiometric signature correlated with the host rock alteration and geometry of the geological unit. Enhanced gridded maps of potassium (K), equivalent thorium (eTh) and equivalent uranium (eU) were produced and subsequently micro-levelled using a routine developed by Blum (1999) (Equivalent Th and U means that the concentration of these two

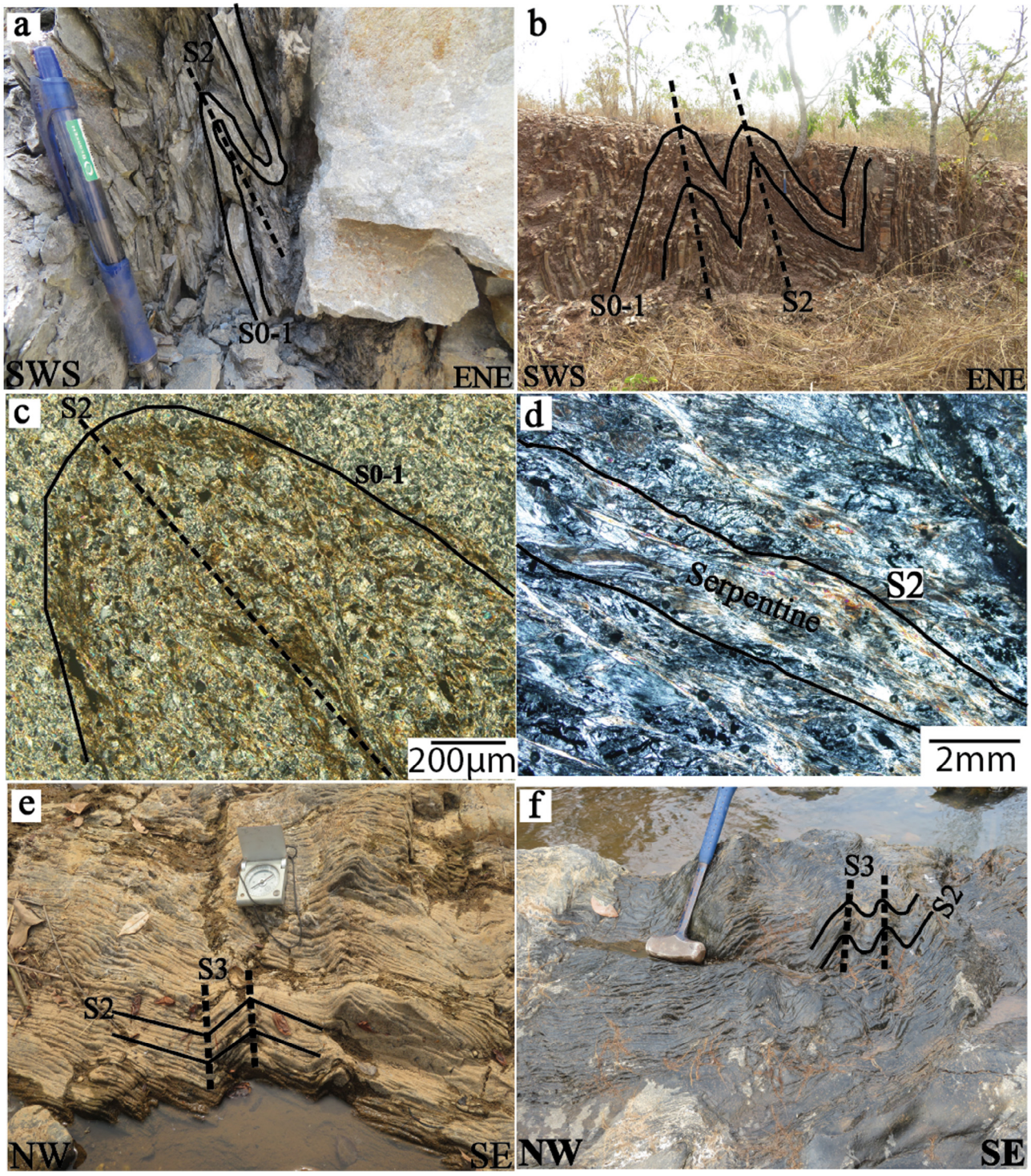

Fig. 4. (a) Field photograph of an isoclinal fold with a steeply east-dipping axial plane parallel to S2 in an interlayer between two sandstone beds of the upper clastic units, (b) field photograph of a F2 chevron fold (slate of the lower clastic units, Fig. 2), which has affected the bedding-parallel S0-1 metamorphic foliation, (c) photomicrograph showing F2 folding of S0-1 metamorphic foliation, with the axial planar schistosity S2 defined by chlorite and/or muscovite (crossed polars), (d) photomicrograph of strongly schistose serpentinite, with the S2 foliation defined by serpentines (crossed polars), (e) and (f) field photographs of (e) F3 kink fold in slate (lower clastic units, Fig. 2), and (f) F3 crenulation of the steep S2 tectonic foliation in chlorite schist.

elements are base on the assumption of equilibrium conditions, thus their radiation is from the decay product of Bi^{214} and Tl^{208}). Micro-levelling filters out most of the seeming residual error left over after the application of the regular survey gridding and also correct for minor inconsistencies, and spatially homogenises the data (Elton et al., 2003). The different histograms of K, eTh, and eU were subjected to histogram equalisation to provide optimal colour disparity (Supplementary Fig. 2a to 2c), before combining to generate the ternary map using Geosoft Oasis Montaj software (Fig. 9). The ternary map is a colour image representing the refined disparities in the ratios of the three radio-elements with K assigned to red, eU to blue and eTh to green.

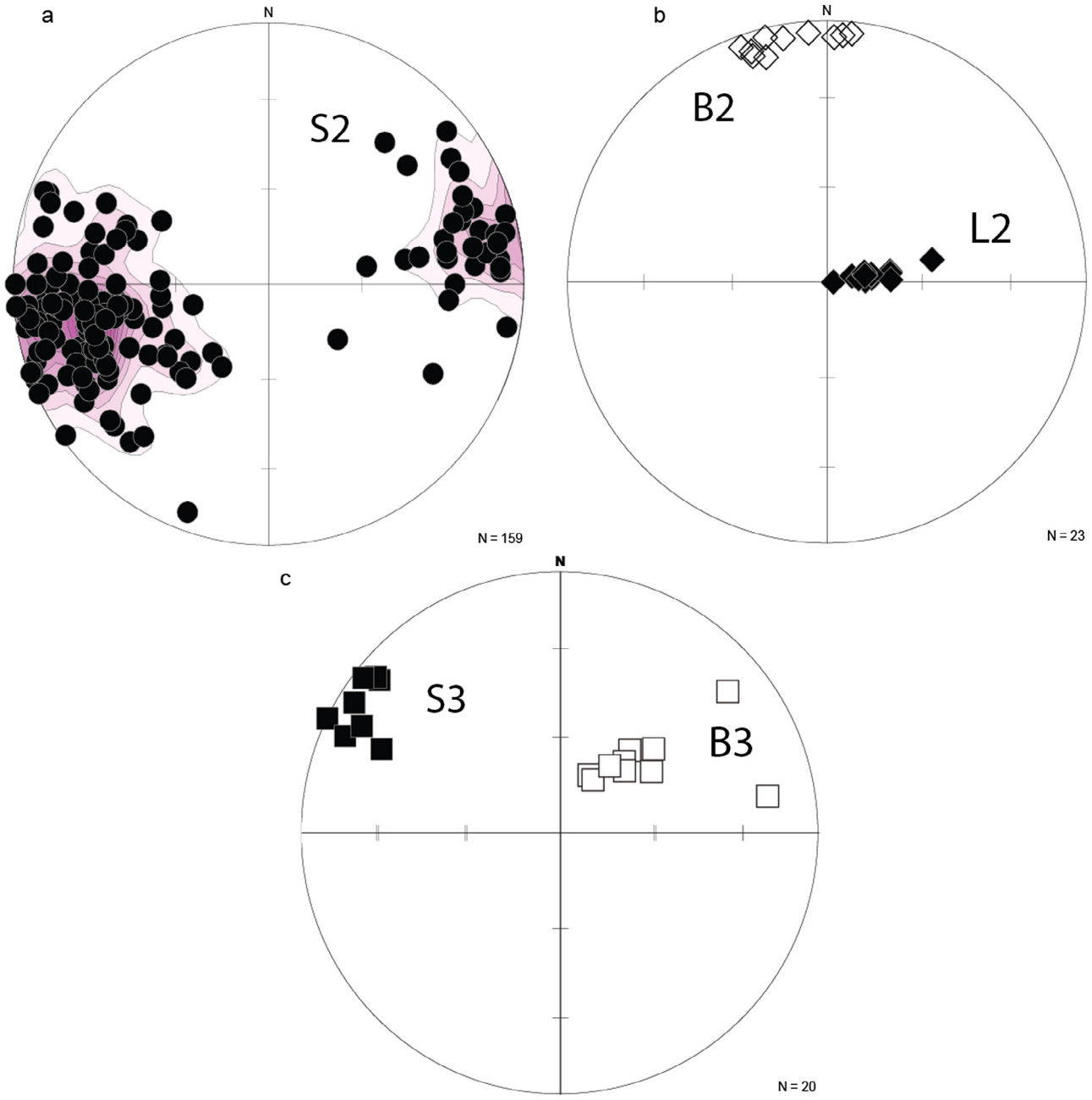

Fig. 5. Lower hemisphere, equal-area plots of poles to foliations and orientation of lineations (a) NNW-striking S2 tectonic foliation, (b) fold axes (open diamonds – B2, shallowly NNW-plunging, filled diamonds – down dip L2 lineations, which plunges to the E-ENE), (c) poles to axial planes of F3 folds (filled squares), B3 fold axis (open squares).

5. Results and interpretation

5.1. Lithological distribution

Magnetic survey is a useful tool in determining the width, depth, and dip of the magnetic body, magnetic susceptibility, and remnant magnetisation by mapping the spatial disparity of the magnetic field strength of the (sub)surface. In regions of stable continental crust, at depth of about 20–25 km, all rocks lose their magnetism (i.e. above the Curie temperature of ca. 550° C; Cook et al., 2003; Purucker and Whaler, 2006). Igneous and metamorphic rocks usually have high magnetic susceptibilities compared to sedimentary rocks.

The spatial dissemination of K, eTh, and eU that is measured during airborne radiometric survey reflects their distribution in the upper 30–45 cm of the crust, and can be used to map horizontal lithological variations, assuming that their distribution in the soil reflects that of the underlying bedrock (Gregory and Horwood, 1961; Wilford et al., 1997).

In the following sections, the lithological distribution and structures observed in the aeromagnetic and radiometric maps are described. Table 1 presents a summary of the major units of the BSU, their mineralogical composition, measured magnetic susceptibility in the field and concentrations of K, eTh, and eU extracted from the airborne radiometric data, general features on the geophysical maps and geological interpretation. A total of 125 rock samples were measured for their magnetic susceptibility (using a handheld SM 30 magnetic susceptibility meter), which ranges from 0.02×10^{-3} SI to 106×10^{-3} SI. The measured susceptibilities were used to distinguish among the various rock units, even though overlaps exist.

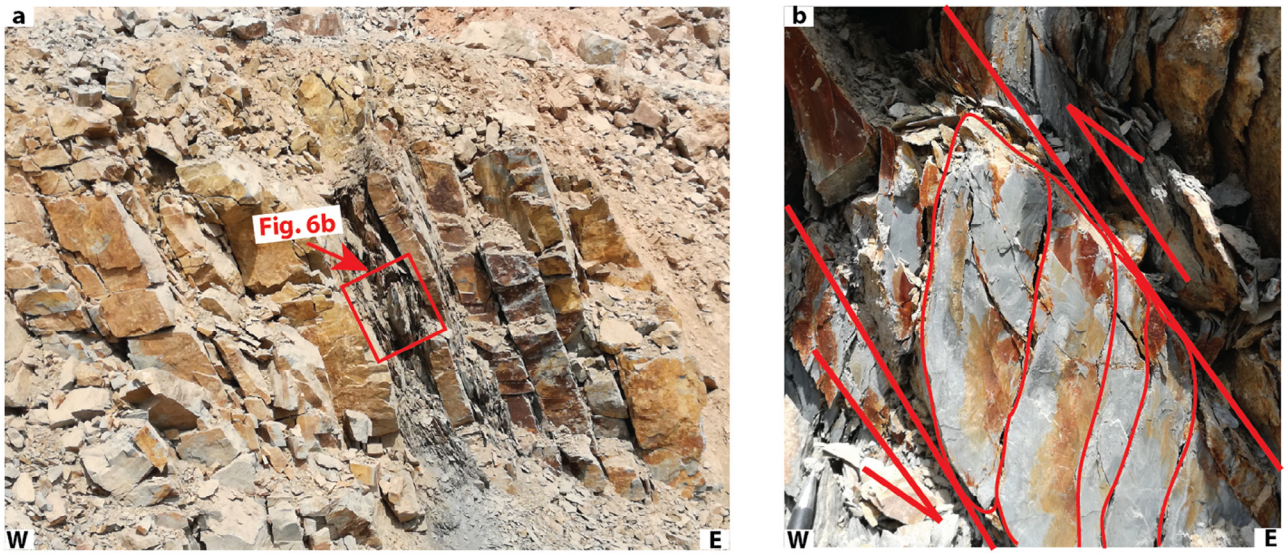

Fig. 6. (a) Field photograph of steeply E-dipping sandstone and slate (upper clastic units, Fig. 2) showing bedding-parallel top-to-the-west D2 shearing, (b) detailled view of the shear zone in Fig. 6a, showing sigmoidal S2 foliation compatible with top-to-the-west sense of shear.

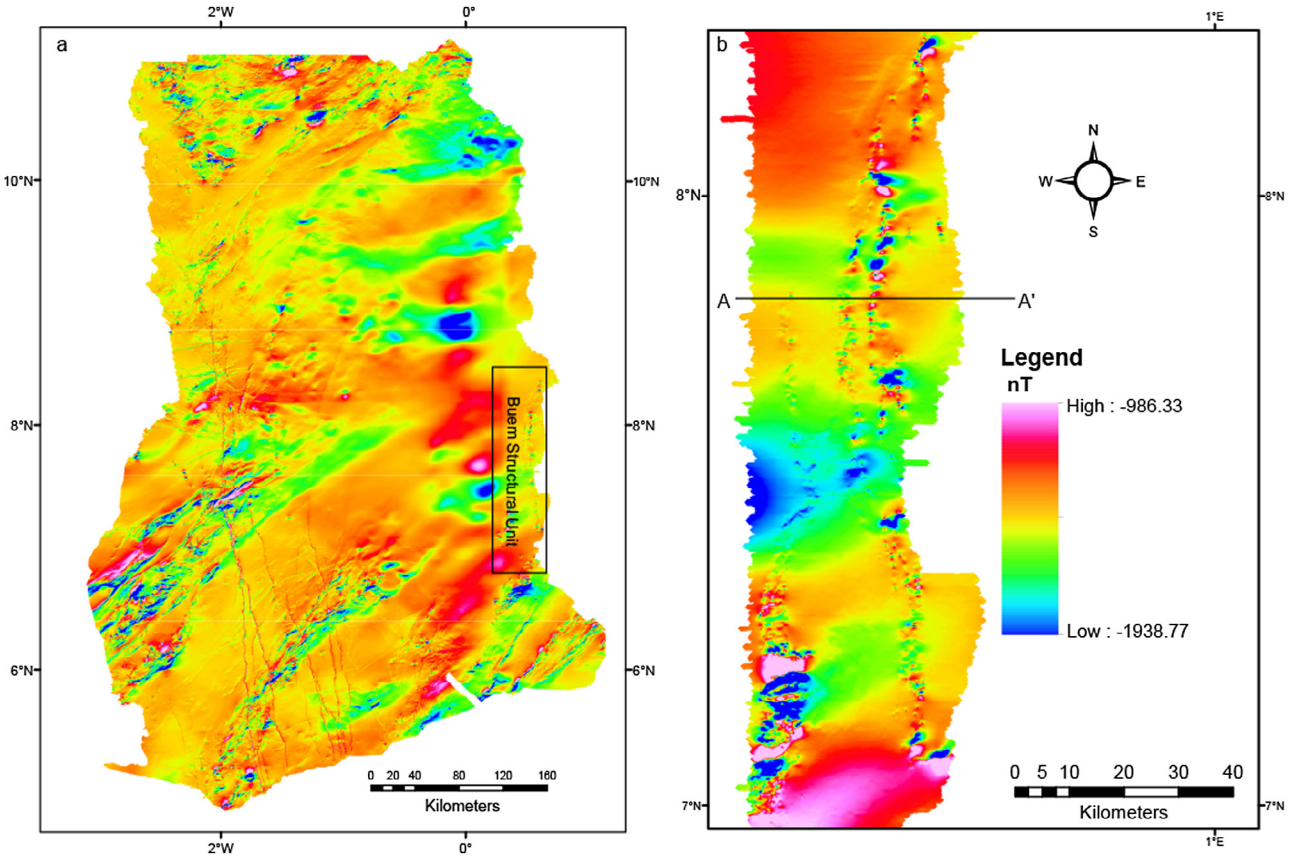

Fig. 7. (a) Total Magnetic Intensity (TMI) map of Ghana showing high and low magnetic intensities of the different geological terrains. The Paleoproterozoic Birimian rocks show NE-SW-trending magmatic highs and low whereas the N-S magnetic high and low anomalies are represented by the Buem Structural Unit. The other N-S linear magnetic anomalies, west of BSU, are mafic dyke swarms (see map in Fig. 1b). (b) TMI map of the BSU. Two sets of magnetic high and low anomalies can be observed: NE-SW- and N-S-trending anomalies. The NE-SW-trending magnetic anomalies are broader and appear to have been superimposed by the N-S magnetic anomalies. The former could correspond to basement rocks of the BSU (i.e. the Paleoproterozoic Birimian rocks).

5.1.1. Volcanic, mafic plutonic and ultramafic rocks

The volcanic rocks of the BSU are basalt, basaltic andesite, trachyte and phonolite with tholeiitic and alkaline signatures, together with pyroclastic rocks (Nude et al., 2015; Kwayisi, 2014). The volcanic rocks generally show medium to high magnetic susceptibility, with the alkaline variety having a higher (1.2–55 $\times$ 10^{-3} SI) susceptibility than the tholeiites (0.02–0.8 $\times$ 10^{-3} SI) and pyroclastic rocks (0.3–17 $\times$ 10^{-3} SI; Table 1). Gabbro and peridotite have medium to high magnetic susceptibilities (0.3–106 $\times$ 10^{-3} SI, and 16–55 $\times$ 10^{-3} SI, respectively; Table 1).

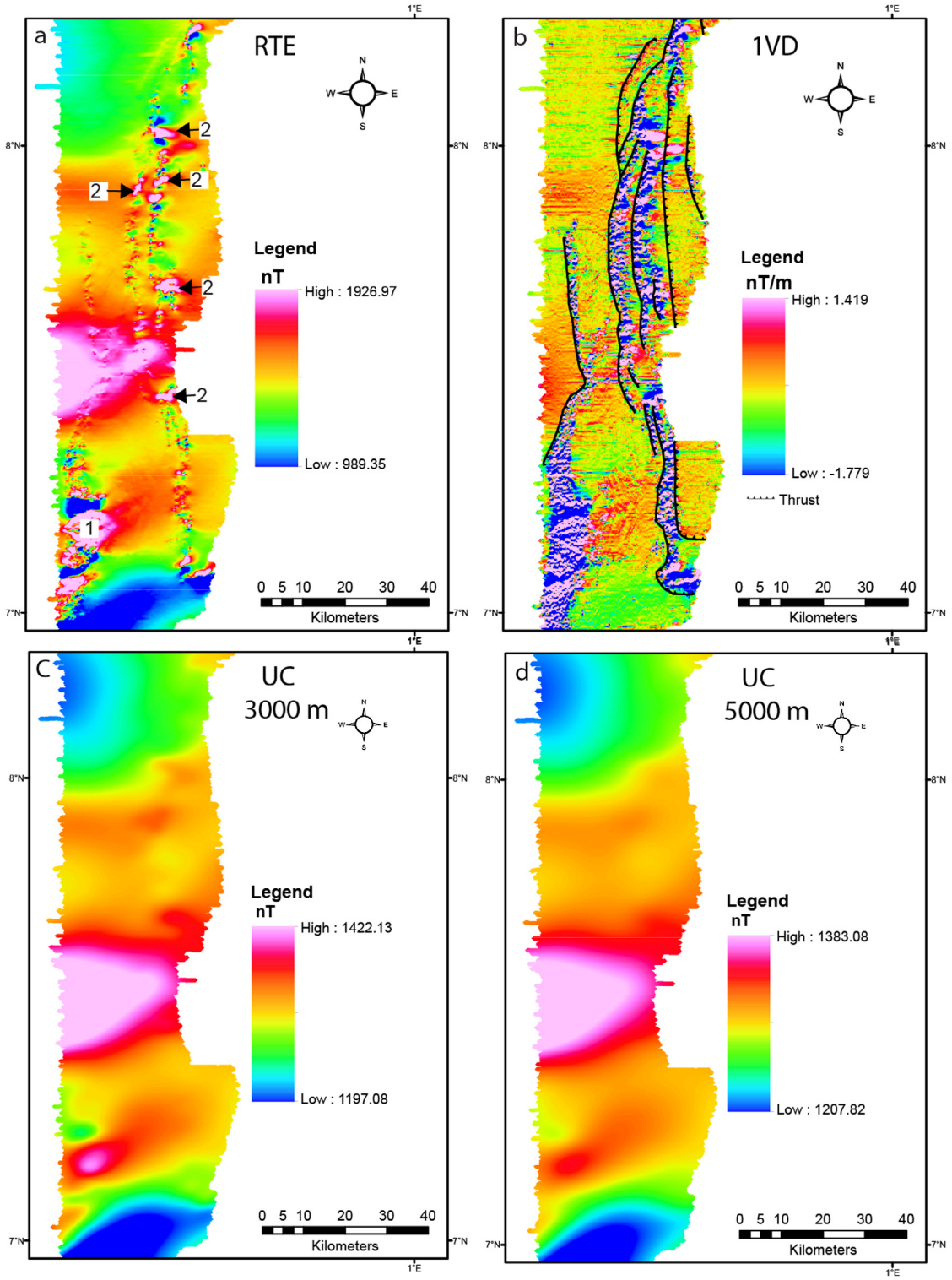

Fig. 8. (a) Reduced-to-the-equator (RTE) aeromagnetic map of the BSU, label 1 on the map represents magnetic highs for the volcanic rocks, and label 2 is for the mafic–ultramafic rocks. (b) First Vertical Derivative (1VD). Major thrust faults have been interpreted based on cyclic map repetition of the same magnetic signal and sharp asymmetric changes on the western side of the magnetic highs. These thrust faults were identified in the field in areas where strongly schistose serpentinites are in contact with or at places overlie the sedimentary rocks. Upward Continuation (UC) maps, (c) Disappearance of the N-S magnetic high and low anomalies, with only very faint traces in the NE part of the BSU in Upward continued magnetic data at a depth of 3000 m, and (d) Upward Continued Magnetic data at 5000 m showing the absence of the N-S magnetic high and low anomalies.

The RTE map for the BSU (Fig. 8a) shows two sets of magnetic anomalies (i.e. ENE-trending long-wavelength (> 1 km) and N-S-trending short wavelength (< 1 km). The N-S-trending magnetic anomalies dominantly show pronounced high-frequency mottled texture typical of volcanic rocks (Cole et al., 2013) although smooth texture can also be observed, whereas the ENE-trending long-wavelength magnetic anomalies show a smooth texture. Correlation with the available geological map, field and SRTM 3 data of the BSU, suggests

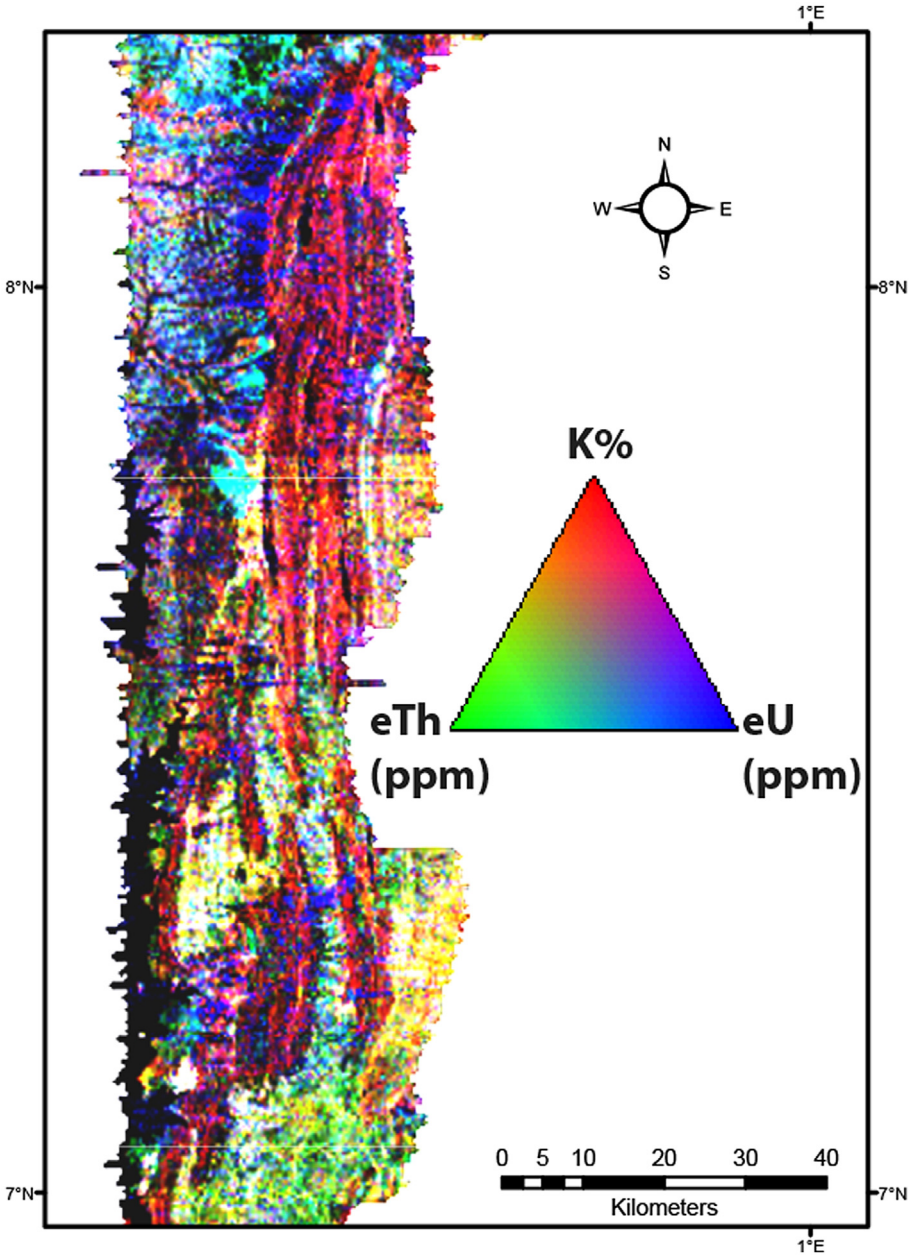

Fig. 9. Ternary map of the study area showing relative distribution of the radioelements. Dark areas represent low concentration of all three radioelements and whitish areas correspond to high concentrations of all three radioelements.

that the volcanic rocks caused the high-intensity magnetic anomalies of the N-S-trending short-wavelength magnetic signal in the western portion of the BSU whereas those located in the eastern part correspond to the presence of the gabbro and peridotite (labelled 1 and 2 in Fig. 8a, respectively). The volcanic rocks were distinguished from the gabbro and peridotite by their typical mottled magnetic texture; however, it was difficult to differentiate the gabbro from the peridotite, as both show smooth high magnetic signals. On the 1VD map (Fig. 8b), there are two N-S-trending belts of high magnetic anomalies corresponding to the volcanic and mafic–ultramafic plutonic rocks of the BSU. Similar trends can also be seen on the analytical signal map (AS; Supplementary Fig. 1a).

The Buem volcanic, and mafic–ultramafic plutonic rocks have very low K contents (< 2%) except for a small portion (2 km^2) at the southwestern corner within the volcanic rocks (labelled × in Supplementary Fig. 2a). Volcanic and mafic–ultramafic plutonic rocks occur in areas of low eTh (< 5 ppm; Supplementary Fig. 2b). A small region of the volcanic rocks at the southwestern corner shows high eTh concentration. This region coincides with high K values on the K map, and this could be because of the presence of highly alkaline volcanic rock type and/or hydrothermal alteration. Lithologies and lithological boundaries that are clearly delineated on the K and eTh maps are not as clear on the eU map (Supplementary Fig. 2c). The relative intensities of K, eTh, and eU were used to generate a ternary map (Fig. 9). The generated ternary map provides the best visualisation of the radiometric intensity that correlates well with the geological features in the area. The volcanic and the mafic–ultramafic plutonic rocks correspond to the dark zones on the ternary map (Fig. 9), indicating low concentrations of K, eTh, and eU.

5.1.2. Sedimentary rocks

The sedimentary rocks of the BSU have low to moderate magnetic susceptibility (0.02–1.3 × 10^{-3} SI). On the magnetic map, the sedimentary rocks exhibit moderate to low magnetic intensities and occupy

most of the BSU (Fig. 8a). The magnetic intensities of the sedimentary rocks are uniform in texture; however, these have been obscured by the adjacent volcanic and mafic–ultramafic plutonic rocks (Fig. 8b and Supplementary Fig. 1a). The various units of the sedimentary rocks (shale, sandstone, diamictite, jasper/chert, and limestone/dolostone) of the BSU are not easily distinguishable on the magnetic maps. Sedimentary and felsic igneous rocks are generally considered to have higher concentrations in radiometric elements than mafic igneous rocks (Ward, 1981; Dickson and Scott, 1997). Accordingly, on the K maps, the high to intermediate K concentrations (3.0–5.0%) occurring ubiquitously in the BSU, correspond to shale and sandstone (Supplementary Fig. 2a). However, the regions of high eTh and eU (5.0–8.0 ppm and 2.5–4.0 ppm, respectively) are occupied by shale, with sandstone occurring in regions of low to intermediate eTh (< 6 ppm) and eU (< 5 ppm; Supplementary Fig. 2b and Fig. 2c). High concentrations of all three elements K, eTh and eU, represented as greenish-white zones (with eTh higher than K and eU; Fig. 9), coincide with shale, confirming that the shale has high concentration of the three radioelements relative to the other sedimentary rocks in the BSU, as shown by geochemical data of Osae et al. (2006). Areas with low eU and eTh, and high K concentrations (shown by magenta colour) corresponds to the Buem sandstone (Fig. 9). The other sedimentary rocks (jasper/chert and limestone/dolostone) were not readily distinguishable on the radioelement maps.

5.2. Inferred geological structures from geophysics

Lineaments, such as faults and thrusts, were inferred from the geophysical maps based on (1) displacement in a prominent linear feature, (2) a sharp change in amplitude, (3) duplication of magnetic signals, (4) truncation of a predominantly linear magnetic domain by a curvilinear feature, and (5) curved magnetic pattern. On the TDR and 1VD maps (Supplementary Fig. 1b and Fig. 8b), several lineaments that have been interpreted as faults and thrusts can be identified. Overall, three main fault orientations have been identified: N-S, E-W and NE-SW faults. Because the N-S magnetic highs are showing (i) cyclic map repetition of the same magnetic signal, (ii) sharp asymmetric changes on their western side and, (iii) a westward-convex shape in map view, they have been interpreted as west-verging thrust planes (Fig. 8b). On the whole, three major thrust systems were identified: at the Voltaian-BSU contact, BSU-TSU contact and sandstone-mafic–ultramafic plutonic rock contacts within the BSU. The occurrence of mafic–ultramafic rocks marks the boundaries of these thrust systems depicted by the geophysics, and this corroborates what has been reported in the literature (Wright et al., 1985; Griffis et al., 2002) and observed in the field (Fig. 10b).

5.3. Depth to the basement of the magnetic source

In Fig. 8a, a conspicuous long-wavelength high and low magnetic anomaly is observed, trending in an ENE direction, which is continuous with and along-strike of the regional structures of the WAC to the west (Fig. 1b and 7a). This may be attributed to a deeper body, probably the basement of the BSU. On the upward continuation map (Fig. 8c and 8d and Supplementary Fig. 1c and Fig. 1d), the N-S-trending short-wavelength high and low magnetic anomalies of the BSU disappear at > 3500 m depth, leaving only the anomalies of the ENE-trending long wavelength. Hence, it can be inferred that the basement rocks of the BSU could be at depth > 3500 m.

The depth to the basement of these ENE-trending magnetic bodies was estimated using the Werner Deconvolution, in one long profile that is orthogonal to the strike of the geological units of the BSU. This technique does not require any initial model for the interpretation (Ku and Sharp, 1983; Jain, 1976; Hartman et al., 1971). Two depth-source models (i.e., dyke and contact) were assumed. In general, 409 and 384 solutions were obtained for dyke and contact respectively, giving a total of 793 solutions. Overall, the profile gave a minimum depth to the basement of 100 m and a maximum depth of 4300 m (Fig. 10). These values are in agreement with the depth to the source of the long-wavelength magnetic anomaly inferred in the upward continuation processing of aeromagnetic data (Fig. 8c and 8d and Supplementary Fig. 1c and Fig. 1d).

6. Discussion

6.1. Tectonostratigraphic record of the BSU

Principal units of the BSU include sandstone, shale, volcanic rocks, gabbro and peridotite all of which have been metamorphosed at lower greenschist facies conditions. According to Junner (1940), the sandstones are strongly folded and steeply dipping whereas the volcanic rocks are less deformed, and dip at a lower angle, thus suggesting that the volcanic rocks of the BSU overlie the sandstones comfortably. Although Crook (1970) agreed with Junner (1940) on the contrasting deformation record between the sandstones and the volcanic rocks, he rather suggested that the sandstones overthrust the volcanic rocks. Conversely, Jones (1990) suggested that the appearance of the sandstone units is not related to tectonic folding but that is an original depositional (pinch-out geometry) feature, representing overlapping alluvial fans. Jones (1990) further argued that folding in the BSU is only confined to the finer-grained horizons (the shales) and that the entire BSU is conformable (i.e. absence of thrust horizons) with the volcanic rocks being the oldest.

Integrated results of our airborne geophysical, field mapping and structural investigations shed new light on the tectonostratigraphic evolution of the BSU (Fig. 11a). First, detailed structural mapping indicates that all the rock units of the BSU have been folded along a near-horizontal NNW-plunging B2 fold axis. Second, we have identified a thrust contact in the field and in the geophysical maps between the Buem sandstone and the Voltaian sandstone further northeast (north of Tutukpene) of the thrust contact shown in the existing geological map (Fig. 1c and Fig. 11a). This shifts the boundary between the BSU and

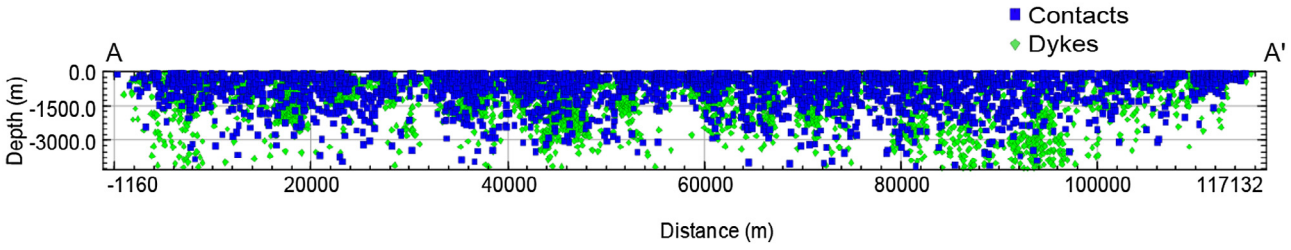

Fig. 10. A total of 793 solutions (409 dyke and 384 contact) of Werner deconvolution from a long profile (A-A') orthogonal to the main strike of the geological units of the BSU (Fig. 7b). Depth estimation models suggest that the source of the body causing these anomalies could be at > 3500 m. Note that the dyke model is generally deeper compared to the contact model. In general, the dyke model have been indicated to occur at deeper depth compared the contact method (Mushayandebvu et al., 2001).

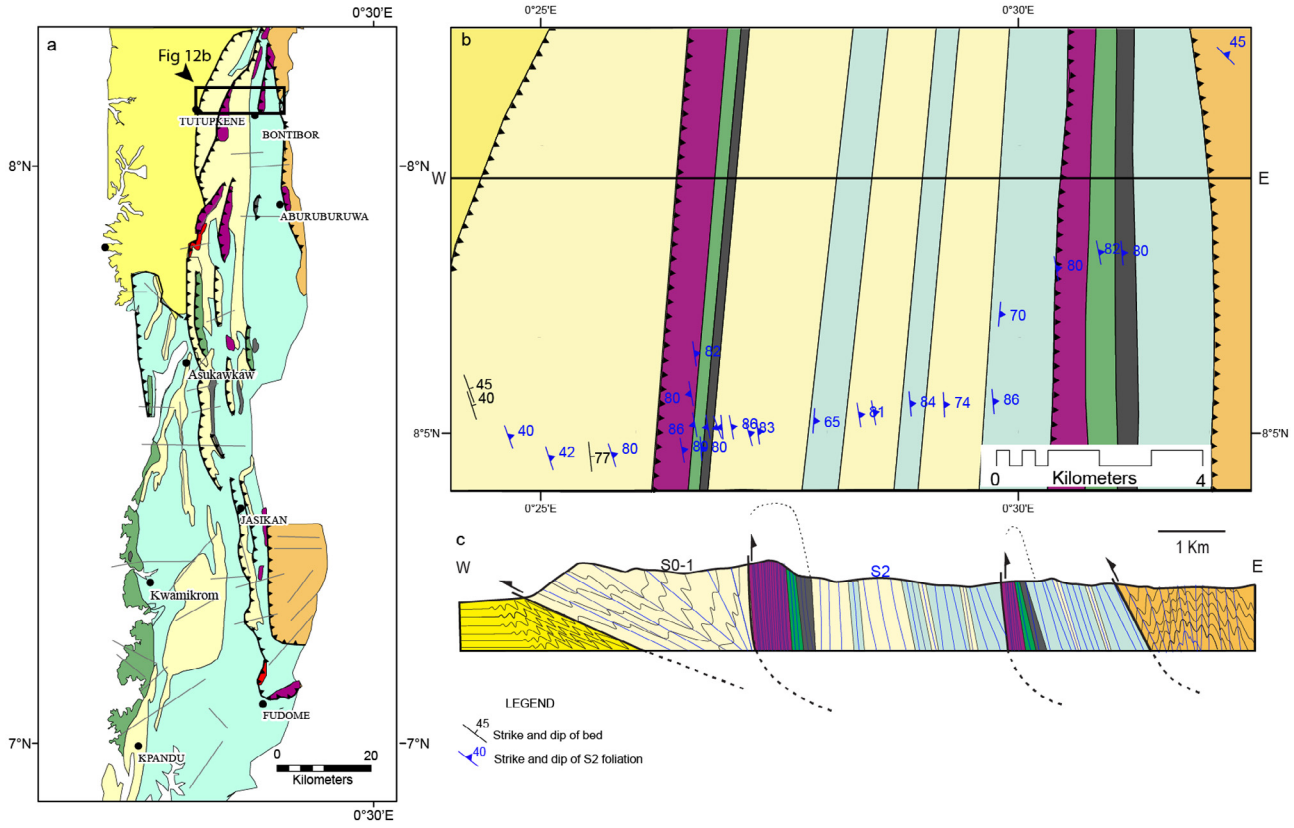

Fig. 11. (a) Interpreted geological map from the aeromagnetic and radiometric data and ground truthing. Note that the mafic/ultramafic and volcanic rocks mark the thrust boundaries between the BSU and Togo Structural Unit/Voltaian Supergroup as well as within the BSU. The detailed investigated area of shown in Fig. 12b is marked by a box. (b) Detailed geological map of a traverse across the BSU fom Tutupkene through Bontibor into the TSU, and (c) a cross-section produced from the Tutupkene-Bontibor traverse. Colour code for maps and cross-section is identical to Fig. 1c.

Voltaian Supergroup further east (≤ 5 km) than previously thought. A similar interpretation of this boundary stems from airborne gravity data (Ayikwei et al., in prep). Third, new occurrences of mafic–ultramafic rocks have been identified, increasing the surface or sub-surface coverage of these rocks by ~ 50% (Fig. 11a). However, it should be noted that a geological map presents a two-dimensional representation of the surface geology, whereas three-dimensional sources influence the geophysical data. Thus, an area with a high magnetic signal can be interpreted as mafic–ultramafic rocks on the geophysical map but, if covered by sediments (non-magnetic body), the field-based geological map will indicate sedimentary rocks such as the upper sandstone unit (Fig. 11a). A similar discrepancy also occurs when the radiometric signal is compared to the aeromagnetic signal. As the radiometric signal is sourced in the top 30 to 40 cm of the earth's surface, areas of volcanic and mafic–ultramafic plutonic rocks depicted in the aeromagnetic map may correspond to high K values in the radiometric map, e.g. sandstones (Fig. 9). Nevertheless, there are many areas where the geophysical signal matches with the surface geology. To the east of the BSU, in the regions of Aburuburuwa and Fodome, ultramafic rocks occur at the boundary between the BSU and the TSU (Fig. 11a). To the west of the BSU, mafic volcanic rocks and mafic–ultramafic plutonic rocks mark the boundary with the Voltaian Supergroup. Within the BSU, some places (e.g. Bontibor) that were mapped as jasper/chert show very high magnetic anomalies, correlated with the occurrence of ultramafic rocks in the field. The magnetic data show that, within the BSU, mafic–ultramafic plutonic rocks mostly occur at the boundary between three main thrust horizons as already noted by Wright et al. (1985), Attoh (1990) and Griffis et al. (2002) based on field observation.

To sum up, our field lithological and structural mapping suggests the following tectono-stratigraphy for the BSU (Fig. 2): The base of the BSU consists of intercalations of slate and *meta*-sandstone, tectonically overlain by peridotite (Fig. 3a and 3b). Nonconformably overlying the peridotite are thin layers of limestone/dolostone and jasper/chert, which in turn are tectonically overlain by gabbro and volcanic rocks (Fig. 3b, 3c, and 3f). Thick beds of intercalated chemical sedimentary units overlie the volcanic rocks (Fig. 3e) with a tectonic contact and are followed by thick sequences of sandstone and diamictite of varied composition (Fig. 2 and Fig. 3h), again in tectonic contact with the underlying rocks.

6.2. Significance of the deformation events

Our detailed field and structural studies indicate that all the units of the BSU have been intensely folded and weakly metamorphosed. Rocks of the BSU generally dip moderately to steeply to the east and occasionally to the west. Three distinct deformation events have been recognised within the BSU. D1 is bedding-parallel, poorly preserved and is observed only in the slate and schist, associated with low-grade metamorphism, defined by albite and sericite. D2 deformation, which is the most pervasive and ubiquitous event, partially to entirely transposed D1 planar fabrics and produced the moderate to steeply ENE-dipping S2 foliation, F2 regional folds, shear zones, and the down-dip, ENE-plunging L2 lineation. Sense of shear indicators, such as the sigmodal foliation associated with down-dip L2 lineation within the D2 shear zones, and the west-verging F2 folds, document a top-to-the west shearing. West-verging thrust planes are compatible with the cyclic repetition, sharp asymmetric magnetic high signals observed in the magnetic maps, and the westward-convex shape of magnetic lineaments in map view (Fig. 8b). Curved thrust belts are typical of progressive oroclines that show convex-shape thrusts in map view towards the direction of movement (e.g. Johnston et al., 2013). Attoh (1998) and Agbossoumonde et al. (2002) proposed that E-W shortening

resulted in the development of N-S-striking and E-dipping structures, in the (U)HP rocks of the PSZ, ~ 50 km east of the BSU (Attoh et al., 2006). This E-W shortening was active around 615–605 Ma and corresponds to the age of HP metamorphism in the PSZ (Affaton et al., 2000, Hirdes and Davis, 2002). It is therefore likely that the dominant N-S-striking and E-dipping S2 cleavage that is ubiquitous in the BSU is related to this E-W shortening active during the Pan-African orogeny at the southeastern margin of the WAC.

Locally, S2 structures are folded by F3 open and kink folds during D3 deformation. D3 deformation may be as a result of a weak NW-SE shortening. D3 fabrics in the BSU might be correlated with the NE-SW-striking fabrics that exhumed the HP rocks in the southern part of the PSZ (Attoh et al., 2007), dated at ~ 587–567 Ma (Ar-Ar ages of hornblende) and 586–578 Ma (U-Pb dating of titanite). The change of orogenic structural grain from N-S to NE-SW trending southwards in the PSZ has been interpreted to be caused by the rotation of the regional tectonic shortening directions from E-W at 615–605 Ma to NW-SE-trending at 587–567 Ma during transition from continental subduction to continent–continent collision (Attoh et al., 1997; 2006). Little is known about the significance of this NW-SE shortening in the PSZ. Castaing et al. (1994) and Toteu et al. (2004) have proposed that it resulted from the collision of the amalgamated WAC-BNS with the Congo Craton at ca. 600–580 Ma. Nevertheless, the shared deformational history between the BSU and the PSZ suggest similar tectonic processes in both domains, marked by continental subduction of the WAC beneath the BNS at 610–605 Ma (Affaton et al., 2000, Hirdes and Davis, 2002), followed by exhumation of the subducted WAC promontory at 580–560 Ma (Attoh et al., 1997; 2006).

6.3. Anatomy of the Buem structural Unit and its implication to the Dahomeyide Orogen

One important observation made from the geophysical data is the conspicuous ENE-trending long-wavelength magnetic anomalies. Depth estimation models suggest that the source of the body causing these anomalies could be at depth > 3500 m. These deep-seated anomalies are broadly parallel to the S3 structures of the BSU; they might, therefore, be interpreted as long-wavelength F3 buckles of a deep and shallow-dipping interface. This possibility may be ruled out because there is no change in orientation of the overlaying N-S-trending magnetic anomalies across the ENE-trending long-wavelength anomalies. Instead, these long-wavelength magnetic anomalies appear continuous with the Paleoproterozoic Birimian structural grain characteristic of the WAC (Fig. 1b and 7a). It is therefore suggested that the WAC underthrust the BSU with a sole thrust at a depth of > 3500 m. This is in agreement with Attoh (1998) and Attoh and Nude (2008) who used field data to suggest that west-directed overthrusting of the BSU and TSU onto the eastern margin of the WAC resulted in nappe stacking and crustal imbrication.

On the 1VD and the TDR maps (Fig. 8b and Supplementary Fig. 1b, respectively), the mafic–ultramafic plutonic rocks appear as tectonic slices, marking the boundary of the thrust sheets within the BSU and at the contact between the BSU and the Voltaian or TSU. The thrusts were identified in the field by juxtaposition and structural repetition of sections of metasedimentary and mafic–ultramafic rocks (Fig. 11b and 11c). Such repetition of metasedimentary and mafic rocks has been observed in other Pan-African belts e.g. the Matchless Amphibolite belt of the Damara Orogen (Meneghini et al., 2017). In the Matchless Amphibolite belt, top-to-the-SE thrusting has been inferred as a result of the juxtaposition and structural repetition of sections of metasediments and metamafic rocks (Meneghini et al., 2017). Massive and pillow basalts (tholeiitic affinity), gabbros, with less common ultramafic bodies, sheeted dykes, and rare lenses of metalimestones and metacherts are preserved within the Matchless Amphibolite belt. These units have been interpreted as a deformed remnant of an ophiolite section (slices of the lower plate) accreted during the Pan-African orogeny (Meneghini et al., 2017). Affaton et al. (1997), Asiedu et al. (2008) and Nude et al. (2015) suggested, based on the geochemical characteristics of the mafic–ultramafic rocks of the BSU, that the BSU is a fragment of oceanic lithosphere, formed in a divergent setting. The BSU is located to the west of the PSZ, and thus could be part of the lower plate stripped off during subduction and accreted onto the southeastern margin of the WAC. Our detailed structural and geophysical studies have indicated that rocks of the BSU underwent a top-to-the-west shearing during D2 deformation with steeply dipping thrust faults (Fig. 11b and 11c). The Lachlan Fold Belt of southeastern Australia shows similar steep dips of thrust faults that flatten at depth over a rigid basement (Glen and VandenBerg, 1987). Accordingly, deformation in the BSU might have occurred during underthrusting of old, rigid continental crust (the Paleoproterozoic Birimian rocks of the WAC) with a major decollement at the base of the BSU.

The occurrence of both shallowly and steeply-dipping fabrics, the rock association (marine and continental) and the location (on the lower plate, along plate margin at the front of the Dahomeyide arc crust, west of the PSZ, suggest that the BSU might have evolved from early accretion of oceanic crust and passive margin sedimentary units to later inversion during closure of an oceanic basin. Detrital zircon ages of the sediments of the BSU indicate the existence of older (younger than 950 Ma; correlated to the passive margin units of the lower Voltaian Supergroup) and younger (600 Ma; correlated to the foreland basin units of the middle Voltaian Supergroup) sediments (Kalsbeek et al., 2008; Ganade de Araujo et al., 2016). This information is crucial, as it suggests the overall evolution of the Dahomeyide Orogen from an initial formation of passive margin sedimentary sequences and mafic–ultramafic magmatic products at or younger than ca. 950 Ma (Kalsbeek et al., 2008), followed by tectonic inversion and deformation (initiation of convergence, ca. 750 Ma; Ganade de Araujo et al., 2016) during the subduction and subsequent collision of the WAC with the BNS (ca. 610 Ma; Ganade de Araujo et al., 2014). Similar geodynamic evolution has been proposed for other Pan-African belts surrounding the WAC: Pharuside/Hoggar belt (Caby, 2003; Liégeois et al., 2003), Anti-Atlas belt (Hefferan et al., 2000, 2002), and Rokelide belt (Villeneuve and Cornée, 1994). It can be concluded that the BSU is an allochthonous fold and thrust belt accreted and thrust onto the southeastern margin of the WAC during the Pan-African orogeny.

Importantly, there are two regions with rocks that share similarities with the BSU within the Trans-Saharan mobile belt in Western Africa and its continuity in Brazil (Fig. 12). First, in northern Mali, the Timétrine massif of the Hoggar-Ifora consists of serpentinized peridotites and ocean-derived assemblages (metavolcanic and chemical sedimentary rocks), which are in close spatial association with passive margin sedimentary rocks (Caby, 2014). Caby (2014) interpreted this association as a typical ocean-continent transition (OCT) ophiolite where sub-continental mantle was exhumed along low-angle detachment faults, followed by the formation of ocean-derived assemblages and passive margin units. Second, in the Novo Oriente Group of the Borborema province, NE Brazil, the occurrence of sheared ultramafic rocks together with metavolcano-sedimentary rocks of passive margin geochemical signature led Granade de Araujo et al. (2010) to propose two distinct scenarios for the formation of these rocks: a magma-poor rifted passive margin or a restricted rift-related basin. This along-strike correlation between the BSU, Timétrine massif and Novo Oriente Group would imply the existence of a discontinuous, 2500 km-long OCT formed during the fragmentation of Rodinia.

7. Conclusion

Integrated structural and airborne geophysical data have been used to delineate magnetic bodies and infer the 3D architecture and tectonic evolution of the BSU. A more substantial occurrence of mafic and ultramafic, and sedimentary rocks occurs within the BSU than previously reported in the literature, which has been affected by three deformation

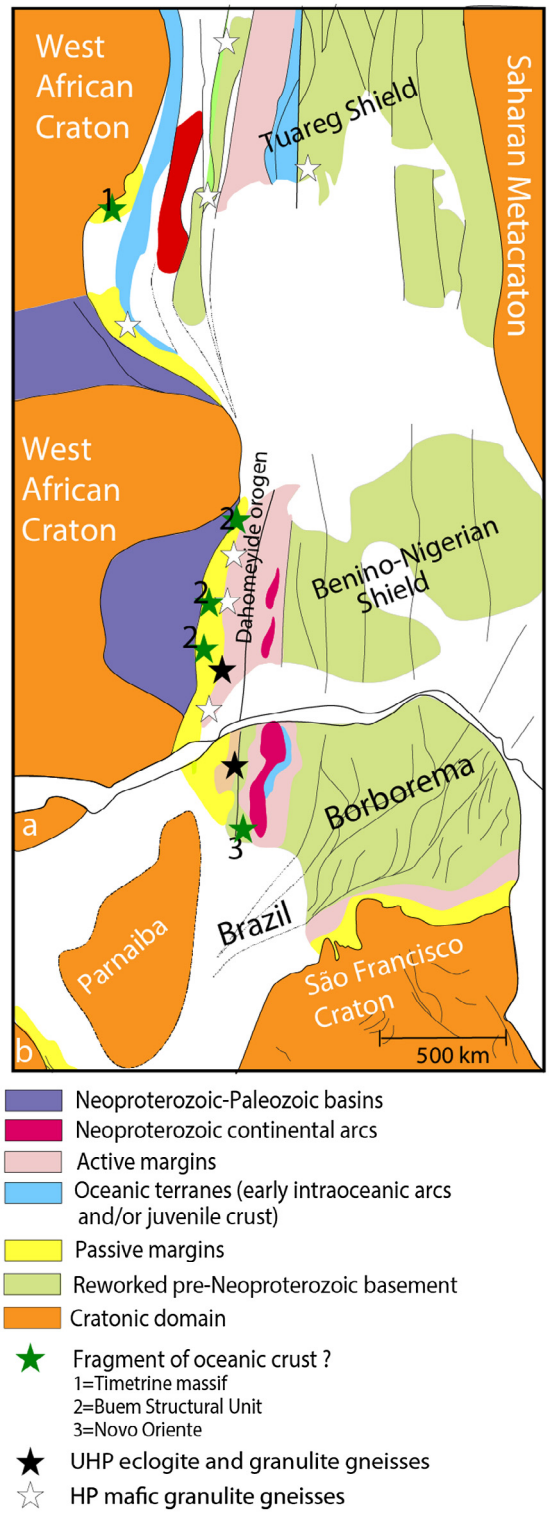

Fig. 12. Regional geological map of West African and Northern Brazil, illustrating the orogen scale of the passive margin and ocean-continent transition within the BSU (Dahomeyide orogen), Timétrine (Hoggar-Iforas), and Novo Oriente group (Borborema province) (Modified after Ganade de Araujo et al., 2014).

events. The main deformational event, D2 reveals top-to-the west shearing, which is attributed to E-W shortening, involving continental subduction and collision during the Pan-African orogeny. Aeromagnetic data are interpreted as showing that the WAC is present under the BSU at depths > 3500 m, implying overthrusting of the BSU onto the WAC. Field relations, structural, aeromagnetic and radiometric data suggest that the entire BSU is a fold and thrust belt, which contains dismembered fragments of oceanic crust. The general tectonic framework of the BSU could suggest that the Pan-African Dahomeyide Orogen might have formed from geological processes involving accretion of mafic–ultramafic rocks and passive margin sedimentary sequences, and their inversion during continent–continent collision. The similarities of the deformation history and rocks association (fragment of oceanic lithosphere) of the BSU with some of the PSZ rocks could connote a genetic relationship. However, major and trace elements, isotopic and geochronological studies are needed to test this hypothesis.

Acknowledgments

The authors are grateful to the Geological Survey Department of Ghana for the release of the airborne geophysical data and vehicle for the fieldwork. This work is supported by the National Research Foundation (NRF) of South Africa grant (105451) awarded to DK, the African-German Network of Excellence in Science (AGNES) Mobility Grant 2018 awarded to DK, Paleoproterozoic Mineralization (PPM) group of the University of Johannesburg, Department of Geology, and DSI-NRF Centre of Excellence for Integrated Mineral and Energy Resource Analysis (CIMERA). The authors would also like to express their gratitude to Mr Emmanuel Nyavor, Mrs Abigail Ayikwei and Ms Stephanie Enslin for their assistance during the fieldwork and/or geophysical data processing. We acknowledge reviews by Jean-Paul Liégeois and one anonimous reviewer as well as editor handling by Professor Wilson Teixeira. This publication presents part of the first author's PhD research.

Appendix A. Supplementary data

Supplementary data to this article can be found online at https://doi.org/10.1016/j.precamres.2019.105568.

References

Affaton, P., 1990. Le bassin des Volta (Afrique de l'Ouest): une marge passive, d'âge protorozoïque suprarieur, tectonisee au Panafricain (600 ± 50 Ma). Etudes et These ORSTOM, Paris, France.

Affaton, P., Aguirre, L., Ménot, R.P., 1997. Thermal and geodynamic setting of the Buem volcanic rocks near Tiéle, Northwest Benin, West Africa. Precambr. Res. 82, 191–209. https://doi.org/10.1016/S0301-9268(97)80686-9.

Affaton, P., Kröner, A., Seddoh, K.F., 2000. Pan-African granulite formation in the Kabye Massif of northern Togo (West Africa): Pb− Pb zircon ages. Int. J. Earth Sci. 88 (4), 778–790. https://doi.org/10.1007/s005310050305.

Affaton, P., Rahaman, M.A., Trompette, R., Sougy, J., 1991. The Dahomeyide Orogen: tectonothermal evolution and relationships with the Volta basin. In: Dallmeyer, R.D., Lecorch_e, J.P. (Eds.), the West African Orogens and Circum- Atlantic Correlatives. Springer, New York, 95-111.

Agbossoumonde, Y., Guillot, S., Menot, R.P., 2004. Pan-African subduction- collision event evidenced by High-P coronas in meta-norites from the Agou Massif (southern Togo). Precambr. Res. 135, 1–21. https://doi.org/10.1016/j.precamres.2004.06.005.

Agbossoumondé, Y., Menot, R.P., Guillot, S., 2002. Metamorphic evolution of Neoproterozoic eclogites from south Togo (West Africa). J. Afr. Earth Sc. 33 (2), 227–244. https://doi.org/10.1016/S0899-5362(01)80061-0.

Asiedu, D.K., Dampare, S.B., Shibata, T., Banoeng Yakubu, B., Osae, S., 2008. The chemical composition and significance of chromian spinels in the Neoproterozoic Anum serpentinites obtained from Anum and Dake-Peki in Southeastern Ghana. J. Ghana Sci. Assoc. 10 (1), 36–43.

Attoh, K., 1982. Structure, gravity models, and stratigraphy of an Early Proterozoic volcanic-sedimentary belt in northeastern Ghana. Precambr. Res. 18, 275–290. https://doi.org/10.1016/0301-9268(82)90014-6.

Attoh, K., 1990. Dahomeyides of Southeastern Ghana: Evidence for oceanic closure and crustal imbrication in a Pan-African orogen. Publication occasionnelle du C.I.F.E.G, BRGM, Orleans Tr, pp. 21.

Attoh, K., 1998. High-pressure granulite facies metamorphism in the Pan-African Dahomeyide orogen, West Africa. J. Geol. 106, 236–246. https://doi.org/10.1086/516019.

Attoh, K., Corfu, F., Nude, P.M., 2007. U-Pb zircon age of deformed carbonatite and alkaline rocks in the Pan-African Dahomeyide suture zone. West Africa. Precambrian Research 155 (3–4), 251–260. https://doi.org/10.1016/j.precamres.2007.02.003.

Attoh, K., Dallmeyer, R.D., Affaton, P., 1997. Chronology of nappe assembly in the Pan-African Dahomeyide orogen, West Africa: evidence from $^{40}Ar/^{39}Ar$ mineral ages.

Precambr. Res. 82, 153–171. https://doi.org/10.1016/S0301-9268(96)00031-9.
Attoh, K., Nude, P.M., 2008. Tectonic Significance of Carbonatite and Ultrahigh-pressure Rocks in the Pan-African Dahomeyide Suture Zone, Southeastern Ghana. Geological Society, London, Special Publications 217–231. https://doi.org/10.1144/SP297.10.
Attoh, K., Samson, S., Agbossoumondé, Y., Nude, P.M., Morgan, J., 2013. Geochemical characteristics and U– Pb zircon LA – ICPMS ages of granitoids from Pan- African Dahomeyide orogen, West Africa. J. Afr. Earth Sc. 79, 1–9. https://doi.org/10.1016/j.jafrearsci.2012.09.015.
Beard, P., 2000. Detection and identification of north-south trending magnetic structures near the magnetic equator. Geophys. Prospect. 48, 745–761. https://doi.org/10.1046/j.1365-2478.2000.00214.x.
Black, R., Caby, R., Moussine-Pouchkine, A., Bertrand, J.M.L., Boullier, A.M., Fabre, J., Lesquer, A., 1979. Evidence for Precambrian plate tectonics in West Africa. Nature 278, 223–227. https://doi.org/10.1038/278223a0.
Black, R., Latouche, L., Liegeois, J.P., Caby, R., Bertrand, J.M., 1994. Pan-African displaced terranes in the Tuareg shield (central Sahara). Geology 22, 641–644. https://doi.org/10.1130/0091-7613(1994) 022<0641:PADTIT>2.3.CO;2.
Blum, M.L.B., 1999. Processamentoe interpretação de dados de geofísica aérea no Brasil central esua plicação à geologia regional e à prospecção mineral. Universidade de Brasília, Brasília, Tese de Doutoramento, Instituto de Geociências, pp. 229.
Burke, K.C., Dewey, J.F., 1972. Orogeny in Africa. In: Dessauvagie, T.F.J., Whiteman, A.J. (Eds.), African Geology. Department of Geology, University of Ibadan, Nigeria, 583–608.
Caby, R., 2014. Nature and evolution of Neoproterozoic ocean-continent transition: Evidence from the passive margin of the West African craton in NE Mali. J. Afr. Earth Sc. 1–11. https://doi.org/10.1016/j.jafrearsci.2013.11.004.
Caby, R., 2003. Terrane assembly and geodynamic evolution of central–western Hoggar: a synthesis. J. Afr. Earth Sc. 37 (3–4), 133–159. https://doi.org/10.1016/j.jafrearsci.2003.05.003.
Castaing, C., Feybesse, J.L., Thieblemont, D., Triboulet, C., Chevremont, P., 1994. Palaeogeographical reconstructions of the Pan-African/Brasiliano orogen: closure of an oceanic domain or intracontinental convergence between major blocks? Precambr. Res. 67, 327–344. https://doi.org/10.1016/0301-9268(94)90095-7.
Castaing, C., Triboulet, C., Feybesse, J.L., Chevremont, P., 1993. Tectonometamorphic evolution of Ghana, Togo and Benin in the light of the Pan-African/Brasiliano orogeny. Tectonophysics 218 (4), 323–342. https://doi.org/10.1016/0040-1951(93)90322-B.
Cole, J., Finn, C.A., Webb, S.J., 2013. Overview of the magnetic signatures of the Palaeoproterozoic Rustenburg layered suite, Bushveld complex, South Africa. Precambr. Res. 236, 193–213. https://doi.org/10.1016/j.precamres.2013.07.017.
Cook, F.A., Lynn, C., Hall, K.W., 2003. Crossstrike potential-field anomalies in the Canadian Cordillera. Can. J. Earth Sci. 40, 1–11. https://doi.org/10.1139/e02-100.
Crook, J.P., 1970. Some preliminary notes on the classification of rocks of eastern Ghana. Ghana Geological Survey Bulletin 38, 27–32.
Dickson, B.L., Scott, K.M., 1997. Interpretation of aerial gamma-ray surveys-adding the geochemical factors. *AGSO* Journal of Australian Geology and Geophysics 17, 187–200.
Duclaux, G., Ménot, R.P., Guillot, S., Agbosoumondé, Y., Hilairet, N., 2006. The mafic-layered complex of the Kabyé massif (north Togo and North Bénin): evidence of a Pan-African granulitic continental arc root. Precambr. Res. 151, 101–118. https://doi.org/10.1016/j.precamres.2006.08.012.
El-Hadj Tidjani, M., Affaton, P., Louis, P., Socohou, A., 1997. Gravity characteristics of the Pan African orogen in Ghana, Togo and Benin (west Africa). J. Afr. Earth Sc. 24 (3), 241–258. https://doi.org/10.1016/S0899-5362(97)00041-9.
Elton, L., Adalene, M., Tati, A., Roberto, A., 2003. Old Geophysical Data Applied to Modern Geological Mapping Problems: A Case-Study in the Seridó Belt. Ne Brazil. Revista Brasileira de'Geociências 33 (2), 65–72.
Ennih, N., Liegeois, J.P., 2001. The Moroccan Anti- Atlas: The West African craton passive margin with limited Pan-African activity. Implications for the northern limit of the craton. Precambr. Res. 112, 291–304. https://doi.org/10.1016/S0301-9268(01)00195-4.
Ennih, N., Liégeois, J.P., 2008. The boundaries of West Africa craton, with a special reference to the basement of the Moroccan metacratonic Anti-Atlas belt. In Ennih, N. and Liégeois, J. p. (Eds). The boundaries of West Africa Craton. Geological Society, London, Special Publications, 297, 1-17.
Ganade de Araujo, C.E., Rubatto, D., Hermann, J., Cordani, U.G., Caby, R., Basei, M.A.S., 2014. Ediacaran 2,500-km-long synchronous deep continental subduction in the West Gondwana Orogen. Gondwana Orogen. Nature Communicaion 5 (5198), 2014. https://doi.org/10.1038/ncomms6198.
Ganade de Araujo, C.E., Cordani, U.G., Agbossoumounde, Y., Caby, R., Basei, M.A., Weinberg, R.F., Sato, K., 2016. Tightening-up NE Brazil and NW Africa connections: New U-Pb/Lu–Hf zircon data of a complete plate tectonic cycle in the Dahomey belt of the West Gondwana Orogen in Togo and Benin. Precambr. Res. 276, 24–42. https://doi.org/10.1016/j.precamres.2016.01.032.
Granade de Araujo, C.E., Pinéo, T.R., Caby, R., Costa, F.G., Cavalcante, J.C., Vasconcelos, A.M., Rodrigues, J.B., 2010. Provenance of the Novo Oriente Group, southwestern Ceará Central Domain, Borborema Province (NE-Brazil): a dismembered segment of a magma-poor passive margin or a restricted rift-related basin? Gondwana Res. 18 (2–3), 497–513. https://doi.org/10.1016/j.gr.2010.02.001.
Ghana National Geological Map Project, 2009. Geological Survey Department of Ghana and Bundesanstalt fur Geowissenschaften und Rohstoffe (BGR), Germany.
Glen, R.A., VandenBerg, A.H.M., 1987. Thin-skinned tectonics in part of the Lachlan Fold Belt near Delegate, southeastern Australia. Geology 15 (11), 1070–1073. https://doi.org/10.1130/0091-7613(1987) 15<1070:TTIPOT>2.0.CO;2.
Gregory, A., Horwood, J., 1961. A laboratory study of gamma-ray spectra at the surface of rocks (No. NP-10937; R-85). Geological Survey of. Department of Mines and Technical. Surveys. Mines Branch, Canada, Ottawa; Canada.
Griffis, R.J., Barning, K., Agezo, F.L., Akosah, F.K., 2002. Gold Deposits of Ghana. Minerals Commission, Accra, Ghana, pp. 432.
Guillot, S., Agbossoumondé, Y., Bascou, J., Berger, J., Duclaux, G., Hilairet, N., Ménot, R.P., Schwartz, S., 2019. Transition from subduction to collision recorded in the Pan-African arc complexes (Mali to Ghana). Precambr. Res. 320, 261–280. https://doi.org/10.1016/j.precamres.2018.11.007.
Gunn, P., 1997. Regional magnetic and gravity responses of extensional sedimentary Basins. AGSO Journal of Australian Geology and Geophysics 17 (2), 115–131.
Guy, A., Schulmann, K., Munschy, M., Miehe, J.M., Edel, J.B., Lexa, O., Fairhead, D., 2014. Geophysical constraints for terrane boundaries in southern Mongolia Journal of Geophysical Research: Solid. Earth 119 (10), 7966–7991. https://doi.org/10.1002/2014JB011026.
Hartman, R.R., Tesky, D.J., Friedberg, J.L., 1971. A system for rapid digital aeromagnetic interpretation. Geophysics 36, 891–918. https://doi.org/10.1190/1.1440223.
Hefferan, K.P., Admou, H., Hilal, R., Karson, J.A., Saquaque, A., Juteau, T., Bohn, M.M., Samson, S.D., Kornprobst, J.M., 2002. Proterozoic blueschist-bearing mélange in the Anti-Atlas Mountains. Morocco. Precambrian Research 118 (3–4), 179–194. https://doi.org/10.1016/S0301-9268(02)00109-2.
Hefferan, K.P., Admou, H., Karson, J.A., Saquaque, A., 2000. Anti-Atlas (Morocco) role in Neoproterozoic Western Gondwana reconstruction. Precambr. Res. 103 (1–2), 89–96. https://doi.org/10.1016/S0301-9268(00)00078-4.
Hirdes, W., Davis, D.W., 2002. U-Pb zircon and rutile metamorphic ages of Dahomeyan garnet-hornblende gneiss in southeastern Ghana, West Africa. J. Afr. Earth Sc. 35 (3), 445–449. https://doi.org/10.1016/S0899-5362(02)00147-1.
Jain, S., 1976. An automatic method of direct interpretation of magnetic models. Geophysics 41, 531. https://doi.org/10.1190/1.1440631.
Geol. Soc. Am. Bull. 125 (5-6), 643–663. https://doi.org/10.1130/B30765.1.
Jones, W., 1990. The Buem volcanic and associated sedimentary rocks, Ghana: a field and geochemical investigation. Journal of African Earth Sciences (and the Middle East),11(3–4), 373–383. https://doi.org/10.1016/0899-5362(90)90016-8.
Junner., N.R., 1940. The Geology of the Gold Coast and western Togoland. Gold Coast Geological Survey Bulletin, 11, 1-40.
Kalsbeek, F., Frei, D., Affaton, P., 2008. Constraints on provenance, stratigraphic correlation and structural context of the Volta basin, Ghana, from detrital zircon geochronology: An Amazonian connection? Sed. Geol. 212 (1–4), 86–95. https://doi.org/10.1016/j.sedgeo.2008.10.005.
Ku, C., Sharp, J., 1983. Werner deconvolution for automated magnetic interpretation and its refinement using Marquart's inverse modeling. Geophysics 48 (6), 754–774. https://doi.org/10.1190/1.1441505.
Kwayisi, D., 2014. Petrology and geochemistry of western Buem volcanic rocks southeastern Ghana: Geodynamic setting implication. MPhil thesis. University of Ghana, Department of Earth Science, pp. 155.
Kwayisi, D., Agra, N.A., Dampare, S.B., Asiedu, D.K., Amponsah, P.O., Nude, P.M., 2017. Two Suites of gabbro in the Buem Structural unit, Southeastern Ghana: Constraints from new field and geochemical data. Journal of African Earth Sciences 129, 45–55. https://doi.org/10.1016/j.jafrearsci.2016.12.018.
Li, X., 2008. Magnetic reduction-to-the-pole at low latitudes: Observations and considerations. Lead. Edge 27, 990–1002. https://doi.org/10.1190/1.2967550.
Liégeois, J.P., Latouche, L., Boughrara, M., Navez, J., Guiraud, M., 2003. The LATEA metacraton (Central Hoggar, Tuareg shield, Algeria): behaviour of an old passive margin during the Pan-African orogeny. J. Afr. Earth Sc. 37 (3–4), 161–190. https://doi.org/10.1016/j.jafrearsci.2003.05.004.
MacLeod, I.N., Jones, K., Dai, T.F., 1993. 3-D Analytic signal in the interpretation of total magnetic field data at low magnetic latitudes. Explor. Geophys. 24, 679–687. https://doi.org/10.1071/EG993679.
Meneghini, F., Fagereng, A., Kisters, A., 2017. The Matchless Amphibolite of the Damara belt, Namibia: unique preservation of a late Neoproterozoic ophiolitic suture. Ofioliti 42 (2), 129–145. https://doi.org/10.4454/ofioliti.v42i2.452.
Milligan, P.R., Gunn, P.J., 1997. Enhancement and presentation of airborne geophysical data. AGSO J. Aust. Geol. Geophys. 17, 63–75.
Mushayandebvu, M., van Drielz, P., Reid, A., Fairhead, J., 2001. Magnetic source parameters of two-dimensional structures using extended Euler deconvolution. Geophysics 66 (3), 814–823. https://doi.org/10.1190/1.1444971.
Nude, P.M., Kwayisi, D., Taki, N.A., Kutu, J.M., Banoeng-Yakubo, C.Y., Anani, B., Asiedu, D.K., 2015. Petrography and chemical evidence for multi-stage emplacement of western Buem volcanic rocks in the Dahomeyide orogenic belt, Southeastern Ghana, West Africa. J. Afr. Earth Sci. 112, 314–327. https://doi.org/10.1016/j.jafrearsci.2015.09.019.
Oruc, B., Selim, H., 2011. Interpretation of magnetic data in the Sinop area of Mid Black Sea, Turkey, using tilt derivative, Euler deconvolution, and discrete wavelet transform. J. Appl. Geophys. 74, 194–204. https://doi.org/10.1016/j.jappgeo.2011.05.007.
Osae, S., Asiedu, D., Banoeng-Yakubo, B., Koeberl, C., Dampare, S., 2006. Provenance and tectonic setting of Late Proterozoic Buem sandstones of southeastern Ghana: Evidence from geochemistry and detrital modes. J. Afr. Earth Sc. 44, 85–96. https://doi.org/10.1016/j.jafrearsci.2005.11.009.
Paine, J.W., 1986. A comparison of methods for approximating the vertical gradient of one dimensional magnetic field data. Geophysics 51 (9), 1725–1735.
Petters, S.W., 2014. Regional geology of Africa. Springer-Verlag, Berlin, pp. 748.
Purucker, M.E., Whaler, K.A., 2006. Crustal magnetism. I M. Kono (Eds.), Elsevier treatise on geophys (Chapter. 5).
Reeves, C., 2005. Aeromagnetic Surveys. Geosoft, e-book, http://www.geosoft.com/knowledge, last accessed 13/12/2010.
Schlueter, T., 2005. Geological atlas of Africa. Springer-Verlag, Berlin, pp. 272.
Toteu, S.F., Penaye, J., Djomani, Y.P., 2004. Geodynamic evolution of the Pan-African

belt in central Africa with special reference to Cameroon. Canadian Journal of Earth Sciences 41 (1), 73–85. https://doi.org/10.1139/e03-079.
Trompette, R., 1997. Neoproterozoic (600 Ma) aggregation of Western Gondwana: a tentative scenario. Precambr. Res. 82, 101–112. https://doi.org/10.1016/S0301-9268(96)00045-9.
Villeneuve, M., Cornée, J.J., 1994. Structure, evolution and palaeogeography of the West African craton and bordering belts during the Neoproterozoic. Precambr. Res. 69 (1–4), 307–326. https://doi.org/10.1016/0301-9268(94)90094-9.
Villeneuve, M., Dallmeyer, R.D., 1987. Geodynamic evolution of the Mauritanides, Bassarides and Rokelides orogens (West Africa). Precambr. Res. 37, 19–28. https://doi.org/10.1016/0301-9268(87)90037-4.
Ward, S.H., 1981. Gamma-ray spectrometry in geologic mapping and uranium exploration. Economic Geology, 75th Anniversary, 840–849.
Wilford, J., Bierwirth, P., Craig, M., 1997. Application of airborne gamma-ray spectrometry in soil or regolith mapping and applied geomorphology. AGSO J. Aust. Geol. Geophys. 17 (2), 201–216.
Wright, J., Hastings, D., Jones, W., Williams, H., 1985. Geology and Mineral Resources of West Africa. George Allen and Unwin publishers Ltd, London, pp. 137.